ARTICLE
Journal of Cellular Biochemistry 112:10–29 (2011)

Journal of Cellular Biochemistry

Stem Cell Property Epithelial-to-Mesenchymal Transition is a Core Transcriptional Network for Predicting Cetuximab (Erbitux™) Efficacy in *KRAS* Wild-Type Tumor Cells

Cristina Oliveras-Ferraros,[1,2] Alejandro Vazquez-Martin,[1,2] Sílvia Cufí,[1,2] Bernardo Queralt,[2,3] Luciana Báez,[2,3] Raquel Guardeño,[2,3] Xavier Hernández-Yagüe,[2,3] Begoña Martin-Castillo,[2,4] Joan Brunet,[2,3] and Javier A. Menendez[1,2*]

[1] *Unit of Translational Research, Catalan Institute of Oncology (ICO), Girona, Spain*
[2] *Girona Biomedical Research Institute (IdIBGi), Girona, Spain*
[3] *Medical Oncology, Catalan Institute of Oncology (ICO), Girona, Spain*
[4] *Unit of Clinical Research, Catalan Institute of Oncology (ICO), Girona, Spain*

ABSTRACT

Beyond a well-recognized effect of *KRAS* mutations in determining de novo inefficacy of cetuximab (CTX) in metastatic colorectal cancer, we urgently need a biomarker signature for predicting CTX efficacy in *KRAS* wild-type (WT) tumors. CTX-adapted *EGFR* gene-amplified *KRAS* WT tumor cell populations were induced by stepwise-chronic exposure of A431 epidermoid cancer cells to CTX. Genome-wide analyses of 44K Agilent's whole human arrays were bioinformatically evaluated by Gene Set Enrichment Analysis (GSEA)-based screening of the KEGG pathway database. Molecular functioning of CTX was found to depend on: (i) The occurrence of a positive feedback loop on Epidermal Growth Factor Receptor (EGFR) activation driven by genes coding for EGFR ligands (e.g., *amphiregulin*); (ii) the lack of a negative feedback on mitogen-activated protein kinase (MAPK) activation regulated by dual-specificity phosphatases (e.g., *DUSP6*) and; (iii) the transcriptional status of gene pathways controlling the epithelial-to-mesenchymal transition (EMT) and its reversal (MET) program (actin cytoskeleton and cell–cell communication—e.g., *keratins*—focal adhesion signaling—e.g., *integrins*—and EMT-inducing cytokines – e.g., transforming growth factor-β). Quantitative real-time PCR, high-content immunostaining, and flow-cytometry analyses confirmed that CTX efficacy depends on its ability to promote: (i) Stronger cell–cell contacts by up-regulating the expression of the epithelial markers E-cadherin and occludin; (ii) down-regulation of the epithelial transcriptional repressors *Zeb*, *Snail*, and *Slug* accompanied by restoration of cortical F-actin; and (iii) complete prevention of the $CD44^{pos}/CD24^{neg/low}$ mesenchymal immunophenotype. The impact of EGFR ligands/MAPK phosphatases gene transcripts in predicting CTX efficacy in *KRAS* WT tumors may be tightly linked with the ability of CTX to concurrently reverse the EMT status, a pivotal property of migrating cancer stem cells. J. Cell. Biochem. 112: 10–29, 2011.

KEY WORDS: CETUXIMAB; EMT; STEM CELLS; KRAS; EGFR LIGANDS

When reviewing the relationship between biomarkers in metastatic colorectal cancer (mCRC) and response to the Epidermal Growth Factor Receptor (EGFR)-targeted monoclonal antibody cetuximab (CTX) [Hawkes and Cunningham, 2010], it becomes clear that, besides the clear-cut deleterious effect of *KRAS* mutations as well as the mutational status of the *KRAS* effector *BRAF* in determining de novo efficacy of CTX in mCRC patients [Wong and Cunningham, 2008; Siena et al., 2009; Bardelli and Siena, 2010], we urgently need novel biomarkers that may predict for the subsequent long-term (LT) outcome and provide a reliable

Conflicts of Interest: Cristina Oliveras-Ferraros received a research salary from a Grant Award by the "Fundacion Salud 2000," which is promoted by Merck Serono (Madrid, Spain). All other authors: None to declare.

Grant sponsor: Ministerio de Sanidad y Consumo, Fondo de Investigación Sanitaria (FIS), Spain; Grant numbers: CD08/00283, CP05-00090, PI06-0778, RD06-0020-0028; Grant sponsor: Ministerio de Ciencia e Innovación (MCINN), Plan Nacional de I+D+I, Spain; Grant number: SAF2009-11579; Grant sponsor: Fundación Científica de la Asociación Española Contra el Cáncer (AECC), Spain.

*Correspondence to: Javier A. Menendez, PhD, Catalan Institute of Oncology, Girona (ICO-Girona), Dr. Josep Trueta University Hospital, Avenida de França s/n, E-17007 Girona, Catalonia, Spain. E-mail: jmenendez@iconcologia.net; jmenendez@idibgi.org

Received 28 October 2010; Accepted 29 October 2010 • DOI 10.1002/jcb.22952 • © 2010 Wiley-Liss, Inc.
Published online 22 November 2010 in Wiley Online Library (wileyonlinelibrary.com).

outcome measure than clinical response criteria alone. Indeed, responses rates to CTX-based therapies remain approximately 40–60% in mCRC patients with *KRAS* and *BRAF* wild-type (WT) tumors [Linardou et al., 2008]. Elucidating mechanisms by which mCRC exhibit de novo refractoriness (i.e., failure of CTX to elicit any detectable response to initial treatment) and acquired auto-resistance (i.e., progression of a mCRC that had previously responded to treatment, despite continued administration of CTX) may be critical to improving the successful clinical management of mCRC patients treated with CTX. Upstream of the CTX target EGFR, the EGFR ligands amphiregulin (AREG) and epiregulin (EREG) have been considered beacons of an activated EGFR pathway and perhaps a necessary positive feedback loop for CTX efficacy. Pharmacogenomic approaches have suggested that, among *KRAS* WT mCRC patients, those expressing higher levels of *AREG* and *EREG* mRNAs are more likely to exhibit a significantly increased responsiveness to CTX [Khambata-Ford et al., 2007; Jacobs et al., 2009]. Downstream of *AREG*, *EREG*, and EGFR, mRNA expression levels of the dual specificity phosphatases (DUSPs) *DUSP4* and *DUSP6*—two mitogen-activated protein kinase (MAPK) phosphatases that promotes a negative feedback loop following MAPK pathway activation [Keise, 2008]—have been suggested also as predictor candidates of outcome after CTX treatment in *KRAS* WT mCRC [De Roock et al., 2009]. Indeed, *DUSP4* and *DUSP6* were originally identified as top resistance markers to CTX in unselected patients and the use of a four-gene expression model, including *AREG*, *EREG*, and *DUSP6* (as well as *SLC26A3* – Solute carrier family 26 member 3) has been shown to improve the identification of responders among pre-selected *KRAS* WT mCRC [Baker et al., 2008]. In this regard, we should expect a significant overlapping between set of genes that are associated with disease control after CTX treatment and sets of genes that are differentially expressed as a function of *KRAS* mutational status (e.g., the EGFR ligand *EREG* as well as the MAPK phosphatases *DUSP4* and *DUSP6*, have been all found to be co-upregulated among the multiple genes induced by several activating *KRAS* mutations in NIH-3T3 fibroblasts) [de Reyniès et al., 2008; Smith et al., 2010].

Recent studies have confirmed a high concordance between the mutation status of *KRAS* and *BRAF* in primary CRC and in corresponding metastases [Gattenlöhner et al., 2009; Italiano et al., 2010; Santini et al., 2010]. The expression (or lack thereof) of other biomarkers should, therefore, actively regulate weaker or stronger responses to CTX. Because molecular mechanisms other than activating *KRAS* mutations should modulate intrinsic (de novo) and secondary (acquired) resistance to CTX in tumors with an intact regulation of *RAS* signaling, we recently envisioned that functional assessing of the transcriptomic signature triggered by CTX before and after CTX-induced chronic prevention of EGFR activation and LT deactivation of EGFR/RAS/MAPK pathway may provide crucial insight into the molecular functioning of the antibody. Taking advantage of two heterogeneous pools of *EGFR* gene-amplified *KRAS* WT A431 tumor cells chronically adapted to grow ($\geq$8 months) in the presence of increasing, clinically relevant doses of CTX, we recently performed genome-wide analyses to definitely establish whether, within a global transcriptomic signature for prediction of response to CTX, the expression status of genes coding for *EGFR* ligands and/or *DUSPs* would be significantly enriched among the several molecular pathways that could associate with the molecular functioning of CTX. Rather than comparing transcriptomic profiles between CTX-naïve parental A431 cells and each A431-derived CTX-adapted A431 POOLs in the absence of CTX treatment (i.e., a transcriptomic signature for CTX resistance), we obtained a global, pathway-focused transcriptomic signature for CTX efficacy by simultaneously comparing global changes in gene expression observed in CTX-treated A431 parental cells and in CTX-treated LT-CTX-adapted A431 POOLs.

Our present experimental approach combined bioinformatic evaluation of multiple genome-wide analyses using Gene Set Enrichment Analysis (GSEA)-based screening of the Kyoto Encyclopedia of Genes and Genomes (KEGG) pathway database with quantitative real-time RT-PCR, high-content immunostaining and flow-cytometry analyses to reveal for the first time that CTX's molecular functioning not only relates to the expression status of *AREG*, *EREG*, and *DUSP* mRNAs as suggested in earlier studies but also to the its ability to prevent the activation of the epithelial-to-mesenchymal transition (EMT) cell differentiation genetic program and, therefore, the occurrence of tumor cell mesenchymal subpopulations with features of cancer stem-like cells and/or the sole presence of stem cell-related features such as the (e.g., integrins- and cytokines-driven) capacity to migrate. If CTX's molecular functioning largely depends on its ability to impede cancer stem cells-like cells to fully assume, in a spontaneous or radiotherapy-/chemotherapy-induced manner, metastasis-facilitating mesenchymal properties, immunohistochemical and/or microarray-based transcriptional profiling studies detecting specific alteration of EMT drivers and/or effectors (and, therefore, an activation of a cancer stem cell gene signature) may be helpful to distinguish responders and nonresponders on the basis of when and where the EMT genetic program becomes activated in tumors treated with CTX.

MATERIALS AND METHODS

DRUGS

The EGFR (HER1)-tyrosine kinase inhibitor (TKI) gefitinib (ZD1839; Iressa®) was kindly provided by AstraZeneca (AstraZeneca PLC Headquarters, 15 Stanhope Gate, W1K 1LN, London, UK). The EGFR (HER1) TKI erlotinib (Tarceva®) was a kind gift from Roche Pharmaceuticals (Neuilly sur Seine, France). The dual HER1/HER2-TKI1 lapatinib (GW572016; Tykerb®) was kindly provided by GlaxoSmithKline (GSK), Corporate Environment, Health and Safety (Brentford, Middlesex, UK). Stock solutions of gefitinib, erlotinib, and lapatinib (10 mM) were prepared in DMSO and stored in aliquots in the dark at −20°C until utilization. Cetuximab (Erbitux®) and trastuzumab (Herceptin®) were kindly provided by Hospital Universitari de Girona Dr Josep Trueta Pharmacy (Girona, Spain). CTX was solubilized with 10 mM NaCl of potassium phosphate buffer (PBS) pH 7.2 in bacteriostatic water for injection purposes (stock solucion at 2 mg/ml), stored at 4°C and used within 1 month. Trastuzumab was solubilized in bacteriostatic water for injection containing 1.1% benzyl alcohol (stock solution at 21 mg/ml), stored at 4°C and used within 1 month. For experimental use, experimental

agents were prepared fresh from stock solutions and were diluted with cell growth medium. Control cells were cultured in media containing identical concentrations (v/v) as the test cells. Vehicle solutions had no noticeable influence on the proliferation of experimental cells.

MATERIALS

Antibodies directed against total and phosphorylation-specific EGFR were obtained from Cell Signaling Technology, Inc. (Danvers, MA). Specifically, we employed the Phospho-EGF Receptor (Tyr1173) (53A5) Rabbit mAb #4407 and the Phospho-EGF Receptor Antibody Sampler Kit #9922 that included: EGF Receptor (D38B1) XP™ Rabbit mAb #4267, Phospho-EGF Receptor (Tyr1068) (D7A5) XP™ Rabbit mAb #3777, Phospho-EGF Receptor (Tyr992) Antibody #2235, Phospho-EGF Receptor (Tyr1045) Antibody #2237 and anti-rabbit IgG, HRP-linked Antibody #7074. Anti-β-actin antibody was purchased from Sigma–Aldrich Co. (St. Louis, MO).

ESTABLISHMENT OF LONG-TERM ACCOMMODATION TO CETUXIMAB IN *EGFR* GENE-AMPLIFIED *KRAS* WT A431 TUMOR CELLS

Over a minimum period of 6 months, cultures of A431 vulvar squamous carcinoma cells (originally obtained from the American Type Culture Collection, Manassas, VA) were continuously exposed to increasing concentrations of CTX. A431 epidermoid carcinoma cells were chosen based on two primary criteria: (1) these EGFR-overexpressing cells are exquisitely sensitive to CTX and (2) A431 cells has not either EGFR Tyrosine Kinase Domain or *KRAS* mutations. Commencing with the IC_{50} of CTX (~25 μg/ml), the exposure dose was progressively increased 2–3 weeks until four-dose doubling had been successfully achieved. Controlled parental cells were cultured in parallel and exposed to the PBS vehicle. We established two LT-CTX-adapted A431 POOLs that were then maintained in continuous culture with the maximal achieved dose of CTX. When challenged to CTX doses as high as 200 μg/ml, they retained a >90% active metabolic status (as assessed by MTT-based cell viability assays – see below) compared to CTX-naïve parental A431 cells (which decreased their ability to metabolize MTT by ~70–80% following treatment with an equivalent dose of CTX; Fig. 1). Parental A431 cells and LT-CTX-adapted POOLs were routinely grown in Dulbecco's Modified Eagle's Medium (DMEM, Gibco® Cell Culture Systems, Invitrogen S.A., Barcelona, Spain) containing 10% heat-inactivated fetal bovine serum (FBS, Bio-Whittaker, Inc., Walkersville, MD), 1% L-glutamine, 1% sodium pyruvate, 50 U/ml penicillin, and 50 μg/ml streptomycin (culture media for LT-CTX-adapted POOLs included 100 μg/ml CTX, which was freshly added during culture splitting). Cells were maintained at 37°C in a humidified atmosphere of 95% air/5% CO_2. Cells were screened periodically for *Mycoplasma* contamination.

METABOLIC STATUS ASSESSMENT (MTT-BASED CELL VIABILITY ASSAYS)

Cells were seeded at a density of ~3,000 cells per well in a 96-well plate. The next day, cells were treated with graded concentrations of CTX, gefitinib, erlotinib, lapatinib, or trastuzumab, as specified. After 5 days of treatment (drugs were not renewed during the entire period of culture treatment), cells were incubated with a solution of MTT [3-(4,5-dimethylthiazol-2-yl)-2,5-diphenyltetrazolium bromide;

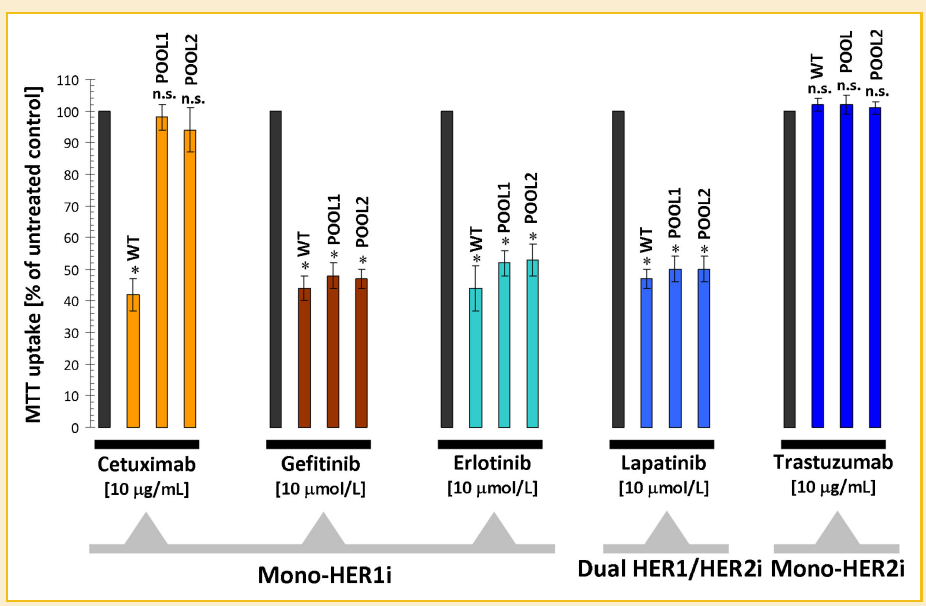

Fig. 1. Characterization of LT-CTX-adapted A431 POOLs relative to parental A431 cells (I): Response to HER1 and/or HER2 targeting drugs. The metabolic status of parental A431 (WT) cells and LT-CTX-adapted A431 POOLs treated with CTX, gefitinib, erlotinib, lapatinib, and trastuzumab was evaluated using a MTT-based cell viability assay and constructing dose–response graphs as percentage of control (untreated) cells (100% MTT uptake). Figure shows means (columns) and 95% confidence intervals (bars) of three independent experiments performed in triplicate (for simplicity figures summarizes the results obtained with one concentration for each drug, as specified). Statistically significant differences (one-factor ANOVA analysis) between experimental conditions and unsupplemented control cells are shown by asterisks ($P < 0.01$) (n.s., no statistically significant; HER1i: HER1 inhibitor; and HER2i: HER2 inhibitor).

Sigma, St. Louis, MO] at a concentration of 5 mg/ml for 3 h at 37°C. The supernatants were then carefully aspirated, 100 μl of DMSO were added to each well, and the plates were agitated to dissolve the crystal product. Absorbances were read at 570 nm using a multi-well plate reader (Model Anthos Labtec 2010 1.7 reader). Cell viability after exposure of cells to drugs was analyzed as percentages of the control cell absorbances, which were obtained from control wells treated with appropriate concentrations of the agents' vehicles that were processed simultaneously. For each treatment, cell viability was evaluated as a percentage using the following equation: (OD_{570} of treated sample/OD_{570} of untreated sample) × 100 (Fig. 1).

IMMUNOBLOTTING PROCEDURES

Cells were washed twice with cold-PBS and then lysed in buffer (20 mM Tris pH 7.5, 150 mM NaCl, 1 mM EDTA, 1 mM EGTA, 1% Triton® X-100, 2.5 mM sodium pyrophosphate, 1 mM β-glycerolphosphate, 1 mM Na_3VO_4, 1 μg/ml leupeptin, 1 mM phenylmethylsulfonylfluoride, and complete protease inhibitor cocktail; Sigma-Chemicals, St. Louis, MO) for 30 min on ice. The lysates were cleared by centrifugation in an Eppendorff tube (15 min at 14,000*g*, 4°C). Protein content was determined against a standardized control using the Pierce Protein Assay Kit (Rockford, IL). Equal amounts of protein (i.e., 50 μg) were resuspended in 5× Laemmli sample buffer (10 min at 70°C), resolved by electrophoresis on 10% SDS-PAGE, and transferred onto nitrocellulose membranes. Non-specific binding on the nitrocellulose filter paper was minimized by blocking for 1 h at room temperature (RT) with TBS-T buffer [25 mM Tris–HCl (pH 7.5), 150 mM NaCl, 0.05% Tween 20] containing 5% (w/v) nonfat dry milk. The treated filters were washed in TBS-T and then incubated with anti-total EGFR or anti-phospho EGFR antibodies, as specified, in 5% (w/v) BSA, 1× TBS-T buffer, 0.1% Tween-20 at 4°C with gentle shaking, overnight. The membranes were washed in TBS-T, horseradish peroxidase-conjugated secondary anti-mouse/rabbit IgGs in TBS-T was added for 1 h, and immunoreactive bands were detected by chemiluminiscence reagent (Pierce Protein Assay Kit). Experiments involving immunoblotting procedures were repeated at least three times and blots were re-probed with an antibody for β-actin to control for protein loading and transfer. Densitometric values of proteins bands were quantified using the Scion Image software (Scion Corporation, Frederick, MD).

SEMI-QUANTITATIVE DETERMINATION OF AKT, Stat3, p38 MAPK, MEK1, AND NF-κB PHOSPHORYLATION STATUS

CST's PathScan® Signaling Nodes Multi-Target Sandwich ELISA Kit#7272 was purchased from Cell Signaling Technology, Inc. This solid phase sandwich ELISA combines the reagents necessary to detect endogenous levels of AKT1, phospho-AKT1 (Ser473), phospho-MEK1 (Ser217/221), phospho-p38 MAPK (Thr180/Tyr182), phospho-Stat3 (Tyr705), and phospho-NF-κB p65 (Ser536). Parental A431 cells and LT-CTX-adapted A431 POOLs (75–80% confluent) were starved overnight and then cultured in the absence or presence of 100 μg/ml CTX in low-serum (0.1% FBS)-containing culture medium for 48 h. Cells were washed twice with cold-PBS and then lysed in buffer (20 mM Tris pH 7.5, 150 mM NaCl, 1 mM EDTA, 1 mM EGTA, 1% Triton® X-100, 2.5 mM sodium pyrophosphate, 1 mM β-glycerolphosphate, 1 mM Na_3VO_4, 1 μg/ml leupeptin, 1 mM phenylmethylsulfonylfluoride, and complete protease inhibitor cocktail; Sigma-Chemicals) for 30 min on ice. The lysates were cleared by centrifugation in an eppendorff tube (15 min at 14,000*g*, 4°C). Protein content was determined against a standardized control using the Pierce Protein Assay Kit. Differential phosphorylation of AKT1, phospho-AKT, phospho-MEK1, phospho-p38 MAPK, phospho-Stat3, and phospho-NF-κB p65 was measured as per manufacturer's instructions. Briefly, after incubation with cell lysates at a protein concentration of 0.5 mg/ml, the target phospho-protein is captured by the antibody coated onto the microwells. Following extensive washing, a detection antibody is added to detect the captured target phospho-protein. An HRP-linked secondary antibody is then used to recognize the bound detection antibody. The HRP substrate TMB is added to develop color. The magnitude of absorbance (measured at 450 nm) for this developed color is proportional to the quantity of bound target protein.

AGILENT GENECHIP ANALYSES

Briefly, total RNA isolated from the CTX-naïve A431 parental cell line and the CTX-accommodated LT-CTX A431 POOLs grown in the absence or presence of 200 μg/ml CTX for 24 h was isolated with TRIzol reagent (Invitrogen, Carlsbad, CA), according to the manufacturer's instructions. RNA quantity and quality were determined using the RNA 6000 Nano Assay kit on an Agilent 2100 BioAnalyzer (Agilent Technologies, Palo Alto, CA), as recommended. Agilent Human Whole Genome Microarrays (G4112F), containing 45,220 probes, were then hybridized. Briefly, 500 ng of total RNA from each sample were amplified by Oligo-dT-T7 reverse transcription and labeled by in vitro transcription with T7 RNA polymerase in the presence of Cy5-CTP or Cy3-CTP using the Quick Amp Labeling Kit (Agilent) and purified using RNAeasy columns (Qiagen). After fragmentation, 825 ng of labeled cRNA from each of the two samples were co-hybridized in in situ hybridization buffer (Agilent) for 17 h at 65°C and washed at RT 1 min in Gene Expression Wash Buffer 1 (Agilent) and 1 min at 37°C in Gene Expression Wash Buffer 2 (Agilent).

STATISTICAL ANALYSIS OF MICROARRAY DATA

The images were generated on a confocal microarray scanner (G2565BA, Agilent) at 5 μm resolution and quantified using GenePix 6.0 (Molecular Dynamics). Spots with signal intensities twice above the local background, not saturated and not flagged by GenePix were considered reliable. Extracted intensities were background-corrected and the $\log_2$ ratios were normalized in an intensity-dependent fashion by the global LOWESS method (intra-chip normalization). Normalized $\log_2$ ratios were scaled between arrays to make all data comparable. Raw data were processed using MMARGE, a web implementation of LIMMA – a microarray analysis library developed within the Bioconductor project in the R statistical environment. To determine genes that were differentially expressed, the multiclass significance analysis of microarrays (SAM) procedure was applied. Probes with q-value (false discovery rate, FDR) below 5% and additionally a fold change exceeding 2.0 in absolute value were initially selected as the relevant ones. Microarray probes were collapsed to genes by taking the median $\log_2$ ratio of the respective probes per gene.

FUNCTIONAL ANALYSIS OF MICROARRAY DATA

To learn more about the biological context of the genes found to be regulated, we applied GSEA. GSEA is a computational method that determines whether an a priori defined set of genes shows statistically significant, concordant differences between two biological states (e.g., phenotypes). The combination of genes commonly regulated in those comparisons was then used as the list of interesting genes. Enrichment of the interesting genes within all available (i.e., 212) KEGG pathways that contained genes present on the used microarray platform was tested with Fisher's exact test. Pathways with q-value (FDR) $<5\%$ were considered as significantly enriched.

FLOW CYTOMETRY

No confluent cultures of parental A431 cells and LT-CTX-adapted A431 POOLs were washed once with phosphate-buffered saline (PBS) and then harvested with 0.05% trypsin/0.025% EDTA into single cell suspensions. Detached cells were washed with PBS containing 1% FBS and 1% penicillin/streptomycin (wash buffer), counted, and resuspended in the wash buffer (10^6 cells/100 μl). Combinations of fluorochrome-conjugated monoclonal antibodies obtained from BD Biosciences (San Diego, CA) against human CD44 (FITC; cat.#555478) and CD24 (PE; cat.#555428) or their respective isotype controls were added to the cell suspension at concentrations recommended by the manufacturer and incubated at 4°C in the dark for 30–40 min. Labeled cells were washed in the wash buffer to eliminate unbound antibody, then fixed in PBS containing 1% paraformaldehyde, and then analyzed no longer than 1 h post-staining on a BD FacScalibur (BD Biosciences).

QUANTITATIVE, REAL-TIME POLYMERASE CHAIN REACTION (qRT-PCR)

Total RNA was extracted from cell cultures of parental A431 cells and LT-CTX-adapted A431 POOLs using a Qiagen RNeasy kit and Qiashredder columns according to the manufacturer's instructions (Qiagen, Valencia, CA). One microgram of total RNA was reverse-transcribed to cDNA using ReactionReady™ First Strand cDNA Synthesis Kit (SABiosciences, Frederick, MD) and applied to EMT PCR Arrays (Cat.#PAHS-090; 96-well format) following SABiosciences RT-PCR manual. Plates were processed in an Applied Biosystems 7500 Fast RT-PCR System Applied Biosystems, Foster City, CA), using automated baseline and threshold cycle detection. Data were interpreted by using SABiosciences' web-based PCR array analysis tool.

IMMUNOFLUORESCENCE STAINING AND HIGH-CONTENT CONFOCAL IMAGING

Cells were seeded at approximately 5,000 cells/well in 96-well clear bottom imaging tissue culture plates (Becton Dickinson Biosciences; San Jose, CA) optimized for automated imaging applications. Triton® X-100 permeabilization and blocking, primary antibody staining (1:50 dilution), secondary antibody staining using Alexa Fluor® 488/594 goat anti-rabbit/mouse IgGs (Invitrogen, Molecular Probes, Eugene, OR) and counterstaining (using Hoechst 33258; Invitrogen) were performed following BD Biosciences protocols. Images were captured in different channels for Alexa Fluor® 488 (pseudo-colored green), Alexa Fluor® 594 (pseudo-colored red) and Hoechst 33258 (pseudo-colored blue) on a BD Pathway™ 855 Bioimager System (Becton Dickinson Biosciences) with 20× or 40× objectives (NA 075 Olympus). Merged images were obtained according to the Recommended Assay Procedure using BD Attovision™ software.

STATISTICS

Two-group comparisons were performed by the Student *t*-test for paired and unpaired values. Comparisons of means of ≥ 3 groups were performed by ANOVA, and the existence of individual differences, in case of significant *F* values at ANOVA, tested by Scheffé's multiple comparisons. In all the cases, statistical analyses were carried out with XLSTAT (Addinsoft™) and $P < 0.01$ was considered to be significant.

RESULTS

CHARACTERISTICS OF A431 EPIDERMOID CANCER CELLS ADAPTED TO GROW IN THE PRESENCE OF CETUXIMAB

Viloria-Petit et al. [2001] pioneeringly reported on the phenotypic changes observed in variants of A431 epidermoid cancer cells that were obtained from recurrent tumor xenografts after two consecutive cycles of therapy with CTX. The sublines established from the relapsed tumors, which reappeared at the site of injection after a prolonged latency period and were refractory to a second round of therapy with CTX, retained high levels of EGFR expression, normal sensitivity to CTX treatment in culture, and an unaltered growth rate, thus indicating that EGFR was not modified on the CTX-refractory tumor cells. Lu et al. [2007], when investigating biochemical changes in signaling pathways of a CTX-resistant subline of DiFi colorectal cancer cells that was developed by exposing the parental sensitive cells to subeffective doses of CTX over an extended period of time, conversely reported that colorectal cancer cells may develop acquired resistance to CTX via altering EGFR levels through promotion of EGFR ubiquitination and degradation (i.e., CTX-resistant DiFi5 colon cancer cells showed marked lower protein levels of EGFR) and using Src kinase-mediated cell signaling to bypass their dependency on EGFR for cell growth and survival. Our current approach was similar to that followed by Lu et al. [2007] as we exposed A431 epidermoid cancer cells to CTX at doses that killed more than 50% of the cells in the first round of treatment and then maintained the surviving fractions of the cells in LT uninterrupted subculture with CTX, gradually increasing the dose of CTX in cell culture. In this scenario aimed to compare congeneic sensitive cells (i.e., parental A431 cells) with counterparts that were experimentally induced to become resistant (i.e., LT-CTX-adapted A431 POOLs) to treatment (i.e., CTX), we decided to follow a conventional approach to identify whether structural or functional changes in the EGFR-driven signaling pathway associated with the occurrence of cell growth adaptation to CTX.

EGFR EXPRESSION AND ACTIVATION STATUS IN LT-CETUXIMAB-ADAPTED A431 POOLS

To evaluate the possibility that loss of the direct CTX target itself (i.e., EGFR) may account for the LT adaptation of A431 cells to grow

in the presence of high-dose CTX, we first performed immunoblotting analyses to determine the expression levels of EGFR before and after the occurrence of unresponsiveness to growth inhibitory effects of CTX. Western blot analysis showed that the total level of EGFR in parental A431 cells was somewhat reduced in A431-derived CTX-adapted A431 POOLs (Fig. 2). Densitometric analyses revealed that EGFR content decreased by ~25% in the POOL1 and by ~40% in the POOL2. These decreased levels of total EGFR in LT-CTX-adapted POOLs relative to parental A431 cells was much lower than that reported by Lu et al. [2007] in their model of acquired resistance to CTX (~80% reduction). Indeed, expression levels of total EGFR in LT-CTX-adapted A431 POOLs were still higher than those observed in colon carcinoma cells known to be sensitive to CTX (data not shown).

EGFR ACTIVATION STATUS IN LT-CETUXIMAB-ADAPTED A431 POOLS

To identify further potential changes in the ability of LT-CTX-adapted tumor cells for transducing EGFR-induced signals to downstream signal mediator/effector molecules as well as for the occurrence of changes in the functional regulation of the EGFR receptor itself, we compared the levels of EGFR tyrosine phosphorylation in parental A431 cells and LT-CTX-adapted A431 POOLs at baseline and on treatment with CTX. We performed immunoblotting procedures with several antibodies recognizing EGFR tyrosine phosphorylation on specific residues [Hynes and Lane, 2005; Citri and Yarden, 2006; Hynes and MacDonald, 2009], including Y992 (phospholipase Cγ-binding site), Y1045 (Cbl-binding site), Y1068 (growth factor receptor binding protein-2 binding site), and Y1173 (together with Y1148 provides a docking site for the Shc scaffold protein, with both sites involved in MAP kinase signaling activation). When information of the relative content of total EGFR was used to adjust the relative level of EGFR phosphorylation in parental A431 cells and LT-CTX-adapted A431 POOLs, LT-CTX-adapted POOLs were found to have lower baseline levels of EGFR phosphorylation on Y992, the sole EGFR tyrosine residue that was significantly inactivated in the presence of CTX. Although EGFR phosphorylation on Y1045 and Y1173 was barely detectable by conventional western blot analysis, CTX exposure significantly induced their phosphorylation in parental A431 cells and LT-CTX-adapted A431 POOLs. Despite lower levels of total EGFR present, LT-CTX-adapted A431 POOLs showed robust phosphorylation on Y1068 upon CTX exposure compared with the residues Y1045 and Y1173. EGFR tyrosine phosphorylation following CTX treatment somewhat differed in parental A431 cells and LT-CTX-adapted A431 POOLs, with deficient phosphorylation on Y992 and more efficient phosphorylation on Y1068 (GRB2-dependent phosphorylation site) in LT-CTX-adapted A431 POOLs. Indeed, LT-CTX-adapted A431 POOLs retained an exquisite sensitivity to the growth-inhibitory effects of the small-molecule mono-EGFR (HER1) TKIs gefitinib and erlotinib and to the dual EGFR/HER2 TKI lapatinib when compared to parental A431 cells (Fig. 2).

INTRACELLULAR SIGNALING NODES IN LT-CETUXIMAB-ADAPTED A431 POOLS

The fact that CTX treatment did not show reduction or even loss of EGFR phosphorylation but rather induction of receptor phosphorylation on Y1045, Y1068, and Y1173 agreed with earlier studies by our and other groups. Mandic et al. [2006] pioneeringly reported that treatment of head and neck squamous cell carcinomas (HNSCC) with CTX paradoxically resulted in enhanced EGFR Y1173 phosphorylation. Yoshida et al. [2008] similarly observed that treatment of nonsmall cell lung cancer (NSCLC) cell lines with CTX-induced phosphorylation of EGFR at several tyrosine phosphorylation sites including Y845, Y1068, and Y1173. Using low-scale phosphor-proteomic approaches we recently reported the ability of CTX to hyper-phosphorylate EGFR in CTX-sensitive MDA-MB-468 breast cancer cells, an in vitro paradigm of intrinsic resistance to EGFR TKIs [Oliveras-Ferraros et al., 2008]. Importantly, the

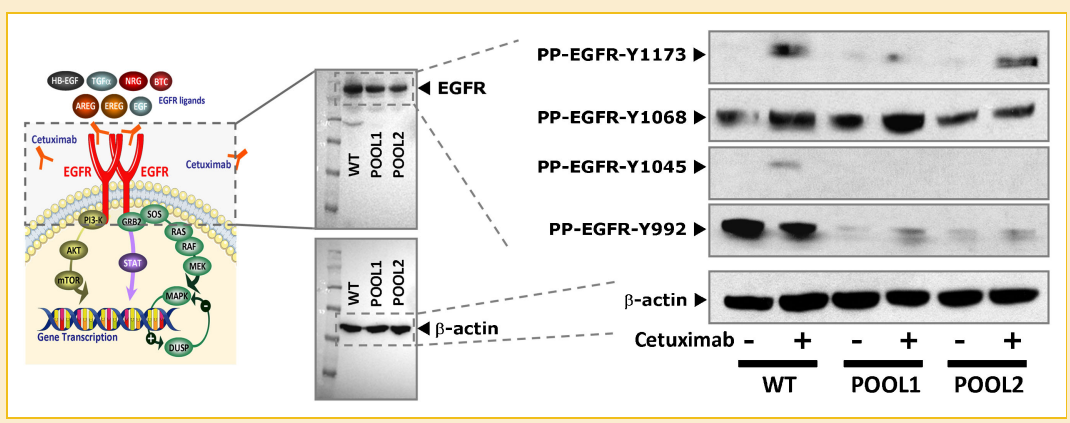

Fig. 2. Characterization of LT-CTX-adapted A431 POOLs relative to parental A431 cells (II): Expression and activation status of EGFR. Left: Decreased levels of total EGFR in LT-CTX-adapted A431 POOLs relative to parental A431 cells. Total levels of EGFR in parental A431 cells and LT-CTX A431 POOLs were compared by subjecting the cell lysates to SDS-PAGE and Western blot analysis with an anti-EGFR antibody. The level of β-actin was used as a reference for cell lysates proteins loaded in the Western blot analysis. Right: Comparison of site-specific phosphorylation of EGFR in parental A431 cells and LT-CTX-adapted A431 POOLs following CTX treatment. A431 and LT-CTX A431 POOLs were treated with 100 μg/ml CTX for 30 min in culture medium with 0.1% FBS. The cells were then lysed and equal amounts of cell lysates were subjected to SDS-PAGE and Western blot analysis with antibodies directed against several site-specific tyrosine-phosphorylated forms of EGFR, as indicated.

above-mentioned studies clearly established that, unlike EGF treatment, CTX-promoted activation of EGFR was not accompanied by activation of the ERK and AKT downstream signaling pathways controlling cancer cell proliferation and survival. Rather, CTX treatment rather fully deactivated ERK and AKT activities [Mandic et al., 2006; Oliveras-Ferraros et al., 2008; Yoshida et al., 2008]. Here, to evaluate the possibility that levels of basal and CTX-regulated phosphorylation of EGFR downstream mediators might mediate loss of CTX functioning in LT-CTX-adapted A431 POOLs, we decided to simultaneously assess the activation status of convergence points and key regulatory proteins in several (EGFR-downstream) signaling pathways controlling cellular events such as growth and differentiation, energy homeostasis, and the response to stress and inflammation.

We took advantage of the CST's PathScan® Signaling Nodes Multi-Target Sandwich ELISA Kit (Cell Signaling Technology, Inc.) to concurrently assess—in a semi-quantitative manner—the endogenous levels of AKT1, phospho-AKT1 (Ser473), phospho-MEK1 (Ser217/221), phospho-p38 MAPK (Thr180/Tyr182), phospho-Stat3 (Tyr705), and phospho-NF-κB p65 (Ser536) in parental A431 cells and CTX-adapted A431 POOLs (Fig. 3). Expression levels of total AKT1 protein were unchanged in A431 POOLs when compared to A431 parental cells and CTX exposure likewise failed to alter total AKT status (data not shown). CTX treatment significantly down-regulated the activation status of AKT1, MEK1, and NF-κB while increasing the activity levels of STAT3. CTX-adapted A431 POOLs displayed a very low phospho-active profile in the convergence signaling points regulated by AKT and MEK1 and somewhat increased NF-κB p65 activity when compared to CTX-sensitive parental A431 cells. CTX treatment failed to significantly alter constitutive low levels of AKT1 and MEK1 in CTX-adapted POOLs. Conversely, CTX exposure increased further the overactive status of NF-κB in CTX-adapted A431 POOLs whereas it reduced NF-κB activity in CTX-sensitive parental A431 cells. Irrespective of CTX treatment, the activation status of p38 MAPK remained unaltered in CTX-adapted POOLs when compared to parental A431 WT cells.

CHARACTERIZATION OF A PATHWAY-BASED TRANSCRIPTOMIC SIGNATURE FOR PREDICTING MOLECULAR FUNCTIONING OF CETUXIMAB

After RNA hybridization to Agilent 44K (double density) Whole Human genome Oligo Microarray (containing 45,220 features—probes—representing 41,000 unique human genes and transcripts), normalized and filtered data from all experimental groups were analyzed simultaneously using the SAM algorithm. We set the significance cut-off at a median FDR of <5.0%. To determine the effects specifically related to CTX efficacy, CTX-induced changes in the transcriptome of CTX-naïve A431 parental cells were compared with the CTX-induced changes in the transcriptome of the two CTX-refractory A431 POOLs. Using a two-fold change cut-off, the transcriptomic signature for CTX efficacy initially included 369 transcriptional effects. When identification of genes that showed significant expression changes was made only considering well-annotated transcripts (not partial *cds* for hypothetical proteins, hypothetical insert cDNA clones, etc.) and genes that could not be identified were rule out, 287 gene transcripts were finally selected for analysis. Tables I and II summarize gene transcripts selectively up- and down-regulated following CTX treatment in CTX-naïve A431 parental cells and in LT-CTX-adapted A431 POOLs, respectively.

To identify functions potentially under selective pressure (i.e., CTX treatment), we used an experimental approach focused on gene pathways instead of outliers. Two methods were applied: GSEA (v2.0, http://www.broad.mit.edu/gsea/)—an algorithm that is oriented

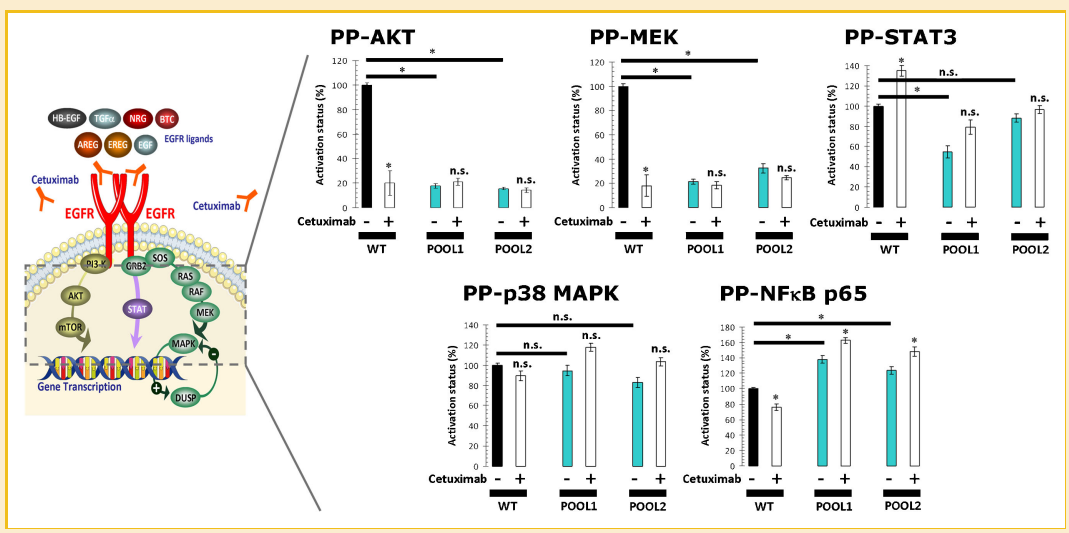

Fig. 3. Characterization of LT-CTX-adapted A431 POOLs relative to parental A431 cells (III): Activation status of intracellular signaling nodes. Lysates from parental A431 cells and LT-CTX-adapted POOLs were assayed at a protein of 0.5 mg/ml using the PathScan® Signaling Nodes Multi-Target Sandwich ELISA Kit#7272 (Cell Signaling Technology, Inc.) as per manufacturer's instructions. The absorbance readings at 450 nm were normalized to those obtained in untreated control cells cultured strictly in parallel. Results are means (columns) and 95% confidence intervals (bars) of two independent experiments made in duplicate. Statistically significant differences (one-factor ANOVA analysis) between experimental conditions groups and/or unsupplemented control cells are shown by asterisks ($P < 0.01$) (n.s., no statistically significant).

TABLE I. Gene Transcripts Differentially Up-Regulated by CTX Treatment in CTX-Naïve Versus CTX-Accommodated *EGFR* Gene-Amplified *KRAS* WT A431 Tumor Cells (Three Independently Performed Microarray Analyses)

ID	Symbol	Entrez gene name	Δ
NM_001946	DUSP6	Dual specificity phosphatase 6	38,728
NM_005438	FOSL1	FOS-like antigen 1	6,690
NM_001964	EGR1	Early growth response 1	6,239
NM_001554	CYR61	Cysteine-rich, angiogenic inducer, 61	6,200
NM_138768	MYEOV	Myeloma overexpressed (in a subset of t(11;14) positive multiple myelomas)	5,881
NM_000575	IL1A	Interleukin 1, alpha	5,695
NM_003897	IER3	Immediate early response 3	4,885
NM_005415	SLC20A1	Solute carrier family 20 (phosphate transporter), member 1	4,630
NM_016639	TNFRSF12A	Tumor necrosis factor receptor superfamily, member 12A	4,460
NM_002228	JUN	Jun oncogene	4,385
NM_001423	EMP1	Epithelial membrane protein 1	4,102
NM_004454	ETV5	Ets variant 5	4,025
NM_001986	ETV4	Ets variant 4	3,955
NM_018948	ERRFI1	ERBB receptor feedback inhibitor 1	3,883
NM_001657	AREG	Amphiregulin	3,765
NM_004073	PLK3	Polo-like kinase 3 (Drosophila)	3,751
NM_030964	SPRY4	Sprouty homolog 4 (Drosophila)	3,740
NM_002526	NT5E	5′-Nucleotidase, ecto (CD73)	3,640
NM_002282	KRT83	Keratin 83	3,597
NM_002607	PDGFA	Platelet-derived growth factor alpha polypeptide	3,510
NM_015993	PLLP	Plasma membrane proteolipid (plasmolipin)	3,477
NM_001993	F3	Coagulation factor III (thromboplastin, tissue factor)	3,469
NM_001394	DUSP4	Dual specificity phosphatase 4	3,431
NM_004431	EPHA2	EPH receptor A2	3,362
NM_002185	IL7R	Interleukin 7 receptor	3,351
NM_001432	EREG	Epiregulin	3,301
NM_003311	PHLDA2	Pleckstrin homology-like domain, family A, member 2	3,226
NM_198277	SLC37A2	Solute carrier family 37 (glycerol-3-phosphate transporter), member 2	3,223
NM_000602	SERPINE1	Serpin peptidase inhibitor, clade E (nexin, plasminogen activator inhibitor type 1), member 1	3,215
NM_004864	GDF15	Growth differentiation factor 15	3,201
NM_001025366	VEGFA	Vascular endothelial growth factor A	3,195
NM_000333	ATXN7	Ataxin 7	3,187
NM_004419	DUSP5	Dual specificity phosphatase 5	3,149
NM_198951	TGM2	Transglutaminase 2 (C polypeptide, protein-glutamine-gamma-glutamyltransferase)	3,105
NM_001945	HBEGF	Heparin-binding EGF-like growth factor	3,090
NM_021972	SPHK1	Sphingosine kinase 1	2,946
NM_002281	KRT81	Keratin 81	2,791
NM_005544	IRS1	Insulin receptor substrate 1	2,777
NM_002213	ITGB5	Integrin, beta 5	2,767
NM_007350	PHLDA1	Pleckstrin homology-like domain, family A, member 1	2,720
AK124869	SH2D5	SH2 domain containing 5	2,718
NM_003088	FSCN1	Fascin homolog 1, actin-bundling protein (Strongylocentrotus purpuratus)	2,715
NM_014508	APOBEC3C	Apolipoprotein B mRNA editing enzyme, catalytic polypeptide-like 3C	2,680
NM_181597	UPP1	Uridine phosphorylase 1	2,665
BC005081	BCAN	Brevican	2,604
NM_005329	HAS3	Hyaluronan synthase 3	2,551
NM_013962	NRG1	Neuregulin 1	2,545
NM_005252	FOS	FBJ murine osteosarcoma viral oncogene homolog	2,520
NM_005429	VEGFC	Vascular endothelial growth factor C	2,509
NM_001004318	PAPL	Iron/zinc purple acid phosphatase-like protein	2,494
NM_003714	STC2	Stanniocalcin 2	2,488
NM_002309	LIF	Leukemia inhibitory factor (cholinergic differentiation factor)	2,480
NM_003786	ABCC3	ATP-binding cassette, sub-family C (CFTR/MRP), member 3	2,467
NM_002467	MYC	v-Myc myelocytomatosis viral oncogene homolog (avian)	2,450
NM_032359	C3ORF26	Chromosome 3 open reading frame 26	2,440
NM_138578	BCL2L1	BCL2-like 1	2,425
NM_000428	LTBP2	Latent transforming growth factor beta binding protein 2	2,420
NM_145298	APOBEC3F	Apolipoprotein B mRNA editing enzyme, catalytic polypeptide-like 3F	2,418
NM_006744	RBP4	Retinol-binding protein 4, plasma	2,398
NM_006779	CDC42EP2	CDC42 effector protein (Rho GTPase binding) 2	2,389
NM_019885	CYP26B1	Cytochrome P450, family 26, subfamily B, polypeptide 1	2,371
NM_144590	ANKRD22	Ankyrin repeat domain 22	2,355
NM_133467	CITED4	Cbp/p300-interacting transactivator, with Glu/Asp-rich carboxy-terminal domain, 4	2,340
NM_004603	STX1A	Syntaxin 1A (brain)	2,330
NM_012099	CD3EAP	CD3e molecule, epsilon associated protein	2,329
NM_006504	PTPRE	Protein tyrosine phosphatase, receptor type, E	2,325
NM_002014	FKBP4	FK506-binding protein 4, 59 kDa	2,312
NM_021784	FOXA2	Forkhead box A2	2,301
NM_021158	TRIB3	Tribbles homolog 3 (Drosophila)	2,295
NM_000224	KRT18	Keratin 18	2,290
NM_173624	FLJ40504	Keratin 18 pseudogene	2,278
NM_003236	TGFA	Transforming growth factor, alpha	2,274
NM_153824	PYCR1	Pyrroline-5-carboxylate reductase 1	2,269

TABLE I. (*Continued*)

ID	Symbol	Entrez gene name	Δ
NM_030567	PRR7	Proline rich 7 (synaptic)	2,264
NM_032463	LAT2	Linker for activation of T cells family, member 2	2,261
NM_006114	TOMM40	Translocase of outer mitochondrial membrane 40 homolog (yeast)	2,255
NM_053056	CCND1	cyclin D1	2,235
AF343078	ATAD3B	ATPase family, AAA domain containing 3B	2,232
NM_016354	SLCO4A1	Solute carrier organic anion transporter family, member 4A1	2,230
NM_001673	ASNS	Asparagine synthetase (glutamine-hydrolyzing)	2,222
NM_022164	TINAGL1	Tubulointerstitial nephritis antigen-like 1	2,220
NM_006142	SFN	Stratifin	2,216
NM_005803	FLOT1	Flotillin 1	2,212
NM_001002259	CAPRIN2	Caprin family member 2	2,211
NM_001005377	PLAUR	Plasminogen activator, urokinase receptor	2,200
NM_153256	C10ORF47	Chromosome 10 open reading frame 47	2,191
NM_006762	LAPTM5	Lysosomal protein transmembrane 5	2,177
NM_002143	HPCA	Hippocalcin	2,152
NM_015169	RRS1	RRS1 ribosome biogenesis regulator homolog (S. cerevisiae)	2,150
BC044637	LOC348926	Family with sequence similarity 86, member A pseudogene	2,146
NM_006037	HDAC4	Histone deacetylase 4	2,126
NM_002205	ITGA5	Integrin, alpha 5 (fibronectin receptor, alpha polypeptide)	2,124
NM_000399	EGR2	Early growth response 2	2,117
NM_032916	FAM86B1	Family with sequence similarity 86, member B1	2,117
NM_014632	MICAL2	Microtubule associated monoxygenase, calponin and LIM domain containing 2	2,114
NM_000147	FUCA1	Fucosidase, alpha-L-1, tissue	2,112
NM_025179	PLXNA2	Plexin A2	2,097
NM_152243	CDC42EP1	CDC42 effector protein (Rho GTPase binding) 1	2,087
NM_017816	LYAR	Ly1 antibody reactive homolog (mouse)	2,084
NM_001759	CCND2	Cyclin D2	2,068
NM_005475	SH2B3	SH2B adaptor protein 3	2,067
NM_018172	FAM86C	Family with sequence similarity 86, member C	2,065
NM_134421	HPCAL1	Hippocalcin-like 1	2,064

to identify sets of functionally related genes and is widely used in the analysis of microarray data [Subramanian et al., 2005]—and over-representation analysis using Fisher's exact test. We began by selecting a set of CTX-regulated genes that were differentially expressed in CTX-naïve and in CTX-adapted tumor cells and, in both analyses, we used the same number of gene sets (i.e., 212) compiled from the KEGG source [Aoki and Kanehisa, 2005]. Thus, GSEA was initially employed to perform a competitive pathway analysis of predefined gene sets in the transcriptomic signature obtained in CTX-treated A431 cells versus CTX-treated LT-CTX A431 POOL1 and in CTX-treated A431 cells versus CTX-treated LT-CTX A431 POOL2. GSEA ranked all genes analyzed by expression arrays according to their differential expression between the two categories of samples and, for each predefined gene set analyzed, the GSEA algorithm calculated a pathway enrichment score that indicated to what extent gene sets were enriched for the highest—or lowest—ranking genes. When enrichment of the interesting genes within all available KEGG pathways that contained genes present on the used microarray platform were tested with Fisher's exact test and pathways with q-value (FDR) $<5\%$ were considered as significantly enriched, we found that 11 enriched gene sets accounted for the differential molecular functioning of CTX in CTX-naïve parental A431 cells versus LT-CTX-adapted A431 POOLs (Fig. 4): *Complement and Coagulation Cascade* (10 genes), *Focal Adhesion* (16 genes), *Cell Communication* (11 genes), *Regulation of Actin Cytoskeleton* (three genes), *ErbB Signaling Pathway* (six genes), *Jak-STAT Signaling Pathway* (9 genes), *Systemic lupus erythematosus* (2 genes), *Cytokine–Cytokine Receptor Interaction* (11 genes), *Colorectal Cancer* (five genes), *MAPK Signaling* (six genes), and *Selenoamino acid metabolism* (four genes).

EPITHELIAL-TO-MESENCHYMAL TRANSITION IS A CRUCIAL GENETIC PROGRAM TARGETED BY CETUXIMAB'S MOLECULAR MECHANISM OF ACTION

Analysis of individual genes within each class of a global transcriptomic signature underlying molecular functioning of CTX confirmed that, in order to fully elicit its growth inhibitory actions against *EGFR* gene-amplified *KRAS* WT A431 tumor cells, the anti-EGFR monoclonal antibody CTX should concomitantly block few signaling pathways, some of which have been separately recognized in earlier studies. First, CTX's molecular functioning appears to largely depend on the occurrence of a high-expression status of genes coding for EGFR ligands (i.e., *AREG*, *HB-EGF*, *NRG*, *TGFA*, and *EREG*). Second, not only CTX-induced inhibition of EGFR ligands expression but also a concomitant down-regulation of the *DUSP*-regulated negative feedback on MAPK activation appears to be necessary for permitting CTX's growth inhibitory effect against EGFR-dependent *KRAS* WT A431 cells. Third, tumor cell entrance to either EMT or the reverse mesenchymal-to-epithelial transition (MET) genetic programs may be pivotal to predict positive tumor response in patients treated with CTX. An important number of genes coding for epithelial differentiation-related cytokeratins including *KRT13*, *KRT14* and *KRT15*, and which down-regulation has been shown to occur in metastatic cells expressing the mesenchymal marker vimentin when compared with their primary vimentin-negative primary (epithelial) counterparts [Paccione et al., 2008], were differentially regulated in response to CTX. Indeed, pivotal players of the EMT program including numerous genes coding for proteins implicated in the regulation of actin cytoskeleton and focal adhesion signaling (e.g., *ITGA5 – integrin α5*, *ITGB5 – integrin β5*, *PDGFA – platelet-derived growth factor A*,

TABLE II. Gene Transcripts Differentially Down-Regulated by CTX Treatment in CTX-Naïve Versus CTX-Accommodated *EGFR* Gene-Amplified *KRAS* WT A431 Tumor Cells (Two Independently Performed Microarray Analyses)

ID	Symbol	Entrez gene name	Δ
NM_006456	ST6GALNAC2	ST6 (alpha-*N*-acetyl-neuraminyl-2,3-beta-galactosyl-1,3)-*N*-acetylgalactosaminide alpha-2,6-sialyltransferase 2	−2,012
NM_014732	KIAA0513	KIAA0513	−2,015
NM_000597	IGFBP2	Insulin-like growth factor binding protein 2, 36 kDa	−2,040
NM_002198	IRF1	Interferon regulatory factor 1	−2,051
NM_018640	LMO3	LIM domain only 3 (rhombotin-like 2)	−2,057
NM_022168	IFIH1	Interferon induced with helicase C domain 1	−2,063
NM_001277	CHKA	Choline kinase alpha	−2,080
NM_001823	CKB	Creatine kinase, brain	−2,088
NM_006379	SEMA3C	Sema domain, immunoglobulin domain (Ig), short basic domain, secreted, (semaphorin) 3C	−2,090
NM_030766	BCL2L14	BCL2-like 14 (apoptosis facilitator)	−2,093
NM_002118	HLA-DMB	Major histocompatibility complex, class II, DM beta	−2,094
NM_020433	JPH2	Junctophilin 2	−2,101
NM_020987	ANK3	Ankyrin 3, node of Ranvier (ankyrin G)	−2,111
NM_001409	MEGF6	Multiple EGF-like-domains 6	−2,114
NM_004669	CLIC3	Chloride intracellular channel 3	−2,116
NM_201553	FGL1	Fibrinogen-like 1	−2,118
BC035246	RIMBP3	RIMS-binding protein 3	−2,140
NM_006813	PNRC1	Proline-rich nuclear receptor coactivator 1	−2,148
AB046765	FBRSL1	Fibrosin-like 1	−2,149
NM_001620	AHNAK	AHNAK nucleoprotein	−2,154
NM_001548	IFIT1	Interferon-induced protein with tetratricopeptide repeats 1	−2,160
NM_020529	NFKBIA	Nuclear factor of kappa light polypeptide gene enhancer in B-cells inhibitor, alpha	−2,166
NM_003151	STAT4	Signal transducer and activator of transcription 4	−2,170
NM_002646	PIK3C2B	Phosphoinositide-3-kinase, class 2, beta polypeptide	−2,173
NM_182908	DHRS2	Dehydrogenase/reductase (SDR family) member 2	−2,180
NM_005532	IFI27	Interferon, alpha-inducible protein 27	−2,183
NM_004925	AQP3	Aquaporin 3 (Gill blood group)	−2,195
NM_002429	MMP19	Matrix metallopeptidase 19	−2,202
NM_032872	SYTL1	Synaptotagmin-like 1	−2,210
NM_006380	APPBP2	Amyloid beta precursor protein (cytoplasmic tail) binding protein 2	−2,210
NM_002053	GBP1	Guanylate-binding protein 1, interferon-inducible, 67 kDa	−2,215
NM_018344	SLC29A3	Solute carrier family 29 (nucleoside transporters), member 3	−2,219
AK055808	C17ORF108	Chromosome 17 open reading frame 108	−2,231
NM_032823	C9ORF3	Chromosome 9 open reading frame 3	−2,240
NM_002737	PRKCA	Protein kinase C, alpha	−2,252
NM_170744	UNC5B	unc-5 homolog B (C. elegans)	−2,257
NM_002964	S100A8	S100 calcium-binding protein A8	−2,260
NM_022074	FAM111A	Family with sequence similarity 111, member A	−2,263
NM_003820	TNFRSF14	Tumor necrosis factor receptor superfamily, member 14 (herpesvirus entry mediator)	−2,267
NM_007197	FZD10	Frizzled homolog 10 (Drosophila)	−2,277
NM_004089	TSC22D3	TSC22 domain family, member 3	−2,280
NM_182915	STEAP3	STEAP family member 3	−2,292
NM_139266	STAT1	Signal transducer and activator of transcription 1, 91 kDa	−2,295
BE825944	STAT2	Signal transducer and activator of transcription 2, 113 kDa	−2,300
NM_003335	UBA7	Ubiquitin-like modifier activating enzyme 7	−2,305
NM_173462	PAPLN	Papilin, proteoglycan-like sulfated glycoprotein	−2,313
AK055918	FLJ31356	Hypothetical protein FLJ31356	−2,317
NM_001008211	OPTN	Optineurin	−2,320
NM_030762	BHLHE41	Basic helix-loop-helix family, member e41	−2,324
NR_001546	TTTY20	Testis-specific transcript, Y-linked 20 (nonprotein coding)	−2,328
NM_002662	PLD1	Phospholipase D1, phosphatidylcholine-specific	−2,333
NM_004848	C1ORF38	Chromosome 1 open reading frame 38	−2,345
NM_017957	EPN3	Epsin 3	−2,349
AK000038	TLCD2	TLC domain containing 2	−2,353
NM_017458	MVP	Major vault protein	−2,353
NM_012465	TLL2	Tolloid-like 2	−2,374
NM_017654	SAMD9	Sterile alpha motif domain containing 9	−2,394
NM_001005291	SREBF1	Sterol regulatory element-binding transcription factor 1	−2,400
NM_003713	PPAP2B	Phosphatidic acid phosphatase type 2B	−2,403
NM_000424	KRT5	Keratin 5	−2,406
NM_016725	FOLR1	Folate receptor 1 (adult)	−2,411
NM_004772	C5ORF13	Chromosome 5 open reading frame 13	−2,414
NM_001953	TYMP	Thymidine phosphorylase	−2,440
NM_001505	GPER	G protein-coupled estrogen receptor 1	−2,445
NM_000624	SERPINA5	Serpin peptidase inhibitor, clade A (alpha-1 antiproteinase, antitrypsin), member 5	−2,451
NM_002065	GLUL	Glutamate-ammonia ligase	−2,453
NM_016817	OAS2	2′-5′-Oligoadenylate synthetase 2, 69/71 kDa	−2,466
NM_020338	ZMIZ1	Zinc finger, MIZ-type containing 1	−2,470
BC068590	CHADL	Chondroadherin-like	−2,470
NM_003153	STAT6	Signal transducer and activator of transcription 6, interleukin-4 induced	−2,475
NR_002802	NEAT1	Nuclear paraspeckle assembly transcript 1 (nonprotein coding)	−2,477
NM_000565	IL6R	Interleukin 6 receptor	−2,485
NM_002146	HOXB3	Homeobox B3	−2,507

TABLE II. (*Continued*)

ID	Symbol	Entrez gene name	Δ
NM_019894	TMPRSS4	Transmembrane protease, serine 4	−2,516
NM_018406	MUC4	Mucin 4, cell surface associated	−2,519
NM_153486	LDHD	Lactate dehydrogenase D	−2,528
NM_001630	ANXA8L2	Annexin A8-like 2	−2,530
NM_002985	CCL5	Chemokine (C-C motif) ligand 5	−2,536
NM_030583	MATN2	Matrilin 2	−2,547
NM_017821	RHBDL2	Rhomboid, veinlet-like 2 (Drosophila)	−2,550
NM_172212	CSF1	Colony stimulating factor 1 (macrophage)	−2,567
NM_182487	OLFML2A	Olfactomedin-like 2A	−2,572
NM_003641	IFITM1	Interferon-induced transmembrane protein 1 (9–27)	−2,584
NM_001001396	ATP2B4	ATPase, Ca++ transporting, plasma membrane 4	−2,587
NM_003004	SECTM1	Secreted and transmembrane 1	−2,603
NM_001003818	TRIM6	Tripartite motif-containing 6	−2,605
NM_004443	EPHB3	EPH receptor B3	−2,605
NM_001007255	KLHDC9	Kelch domain containing 9	−2,628
NM_001352	DBP	D site of albumin promoter (albumin D-box) binding protein	−2,633
NM_058186	FAM3B	Family with sequence similarity 3, member B	−2,680
M32220	LOC441869	Hypothetical protein LOC441869	−2,694
NM_032855	HSH2D	Hematopoietic SH2 domain containing	−2,701
BC093991	HSPB9	Heat shock protein, alpha-crystallin-related, B9	−2,711
BC001196	HS6ST1	Heparan sulfate 6-*O*-sulfotransferase 1	−2,718
NM_199461	NANOS1	Nanos homolog 1 (Drosophila)	−2,719
NM_001262	CDKN2C	Cyclin-dependent kinase inhibitor 2C (p18, inhibits CDK4)	−2,725
NM_002776	KLK10	Kallikrein-related peptidase 10	−2,729
NM_020168	PAK6	p21 protein (Cdc42/Rac)-activated kinase 6	−2,752
NM_001124	ADM	Adrenomedullin	−2,755
AK096661	NEURL1B	Neuralized homolog 1B (Drosophila)	−2,762
NM_022124	CDH23	Cadherin-related 23	−2,762
NM_030899	ZNF323	Zinc finger protein 323	−2,780
NM_006074	TRIM22	Tripartite motif-containing 22	−2,785
NM_031458	PARP9	Poly (ADP-ribose) polymerase family, member 9	−2,829
NM_020639	RIPK4	Receptor-interacting serine-threonine kinase 4	−2,830
NM_033086	FGD3	FYVE, RhoGEF and PH domain containing 3	−2,831
NM_016582	SLC15A3	Solute carrier family 15, member 3	−2,887
NM_021101	CLDN1	Claudin 1	−2,900
NM_001003940	BMF	Bcl2 modifying factor	−2,940
NM_001710	CFB	Complement factor B	−2,943
NM_022147	RTP4	Receptor (chemosensory) transporter protein 4	−2,948
NM_130469	JDP2	Jun dimerization protein 2	−2,957
NM_199511	CCDC80	Coiled-coil domain containing 80	−2,975
NM_054111	IP6K3	Inositol hexakisphosphate kinase 3	−2,976
NM_014353	RAB26	RAB26, member RAS oncogene family	−2,980
NM_006291	TNFAIP2	Tumor necrosis factor, alpha-induced protein 2	−2,991
NM_004079	CTSS	Cathepsin S	−3,001
NM_001013398	IGFBP3	Insulin-like growth factor binding protein 3	−3,095
NM_032587	CARD6	Caspase recruitment domain family, member 6	−3,097
NM_005564	LCN2	Lipocalin 2	−3,142
NM_000246	CIITA	Class II, major histocompatibility complex, transactivator	−3,145
NM_006084	IRF9	Interferon regulatory factor 9	−3,147
NM_003782	B3GALT4	UDP-Gal:betaGlcNAc beta 1,3-galactosyltransferase, polypeptide 4	−3,165
NM_005764	PDZK1IP1	PDZK1 interacting protein 1	−3,195
NM_002315	LMO1	LIM domain only 1 (rhombotin 1)	−3,226
NM_053025	MYLK	Myosin light chain kinase	−3,230
NM_002534	OAS1	2′,5′-Oligoadenylate synthetase 1, 40/46 kDa	−3,261
NM_182909	FILIP1L	Filamin A interacting protein 1-like	−3,305
NM_016618	KRCC1	Lysine-rich coiled-coil 1	−3,309
NM_000104	CYP1B1	Cytochrome P450, family 1, subfamily B, polypeptide 1	−3,352
NM_052941	GBP4	Guanylate-binding protein 4	−3,455
NM_004428	EFNA1	Ephrin-A1	−3,490
NM_152703	SAMD9L	Sterile alpha motif domain containing 9-like	−3,493
NM_005557	KRT16	Keratin 16	−3,501
NM_014398	LAMP3	Lysosomal-associated membrane protein 3	−3,612
NM_203339	CLU	Clusterin	−3,670
NM_153840	GPR110	G protein-coupled receptor 110	−3,733
NM_004120	GBP2	Guanylate-binding protein 2, interferon-inducible	−3,792
NM_017523	XAF1	XIAP associated factor 1	−3,800
NM_013289	KIR3DL1	Killer cell immunoglobulin-like receptor, three domains, long cytoplasmic tail, 1	−3,828
NM_006163	NFE2	Nuclear factor (erythroid-derived 2), 45 kDa	−3,881
BC090889	AHNAK2	AHNAK nucleoprotein 2	−4,003
NM_152673	MUC20	Mucin 20, cell surface associated	−4,101
NM_006472	TXNIP	Thioredoxin interacting protein	−4,150
NM_022748	TNS3	Tensin 3	−4,197
NM_001733	C1R	Complement component 1, r subcomponent	−4,213
NM_009587	LGALS9	Lectin, galactoside-binding, soluble, 9	−4,294
NM_002974	SERPINB4	Serpin peptidase inhibitor, clade B (ovalbumin), member 4	−4,353

TABLE II. (*Continued*)

ID	Symbol	Entrez gene name	Δ
NM_019089	HES2	Hairy and enhancer of split 2 (Drosophila)	−4,388
NM_033285	TP53INP1	Tumor protein p53 inducible nuclear protein 1	−4,436
BC042557	C11ORF93	Chromosome 11 open reading frame 93	−4,461
NM_007021	C10ORF10	Chromosome 10 open reading frame 10	−4,516
NM_022873	IFI6	Interferon, alpha-inducible protein 6	−4,587
NM_207429	C11ORF92	Chromosome 11 open reading frame 92	−4,736
NM_138434	C7ORF29	Chromosome 7 open reading frame 29	−4,861
NM_001734	C1S	Complement component 1, s subcomponent	−4,867
NM_003695	LY6D	Lymphocyte antigen 6 complex, locus D	−4,907
NM_014033	METTL7A	Methyltransferase-like 7A	−4,910
NM_006113	VAV3	Vav 3 guanine nucleotide exchange factor	−4,920
NM_002463	MX2	Myxovirus (influenza virus) resistance 2 (mouse)	−4,970
NM_003106	SOX2	SRY (sex determining region Y)-box 2	−5,205
NM_030761	WNT4	Wingless-type MMTV integration site family, member 4	−5,345
NM_002276	KRT19	Keratin 19	−5,386
NM_002423	MMP7	Matrix metallopeptidase 7 (matrilysin, uterine)	−5,520
NM_002462	MX1	Myxovirus (influenza virus) resistance 1, interferon-inducible protein p78 (mouse)	−5,564
NM_006235	POU2AF1	POU class 2 associating factor 1	−5,679
NM_006820	IFI44L	Interferon-induced protein 44-like	−5,965
NM_152908	SLC47A2	Solute carrier family 47, member 2	−6,083
NM_006919	SERPINB3	Serpin peptidase inhibitor, clade B (ovalbumin), member 3	−6,207
AK000177	MCM9	Minichromosome maintenance complex component 9	−6,413
NM_058229	FBXO32	F-box protein 32	−6,623
NM_004433	ELF3	E74-like factor 3 (ets domain transcription factor, epithelial-specific)	−7,223

PDGFB – platelet derived growth factor B) and prototypical cytokines for induction of EMT including Transforming Growth Factor (*TGF*)-*β* [Bates, 2005; Gotzmann et al., 2006; Cicchini et al., 2008; Bianchi et al., 2010] were found in the transcriptomic signature predicting for CTX efficacy. In this scenario, we decided to explore further whether there was a programmed series of gene events controlling EMT and/or stem cell biology that could explain molecular functioning of CTX, as suggested by the transcriptomic signature.

RNA from parental A431 cells and LT-CTX-adapted A431 POOLs were evaluated using qRT-PCR of genes specifically associated with EMT and the reciprocal mesenchymal-to-epithelial transition (MET). When a 2-fold or greater difference in mRNA expression levels was used as the cut-off to determine significant regulatory effects on genes involved in the EMT program, LT-CTX-adapted A431 POOLs were found to down-regulate a total of 15 (18%) and to up-regulate a total of 10 (12%) of the 84 EMT gene-regulators assessed in the experiment (Fig. 5). Tumor cells chronically adapted to grow in the continuous presence of CTX transcriptionally repressed the expression of developmental EMT genes that have been repeatedly demonstrated to play pivotal roles in malignant progression: *ZEB1*, *ZEB2*, *SNAI1*, and *SNAI2* (*Slug*) [Peinado et al., 2007; Moreno-Bueno et al., 2008, 2009]. Indeed, CTX-adapted tumor cells negatively regulated the expression of the pleiotropic cytokine TGFβ1, a major driving force of the EMT genetic program (Moustakas and Heldin, 2007; Mani et al., 2008; Massagué 2008; Thiery et al., 2009; Wharton and Derynck, 2009; Singh and Settleman, 2010]. Accordingly, LT-CTX-adapted A431 POOLs notably decreased the expression of plasminogen activator inhibitor type-1 (PAI-1; SERPINE1), a prominent member of the subset of TGFβ1-initiated EMT-related signaling events [Samarakoon et al., 2009; Freytag et al., 2010] and the mesenchymal marker vimentin [*VIN*; Kokkinos et al., 2007]. Importantly, down-regulation of EMT drivers and effectors was accompanied by the significant up-regulation of genes coding for cytokeratins of the epithelial lineage (e.g., *KRT17* and *KRT19*) and for the well-recognized epithelial markers E-cadherin (*CDH1*) and occludin (*OCLN1*). Supporting the notion that chronic sub-culturing in the presence of CTX appears to efficiently prevent the occurrence of EMT-like phenomena at the transcriptional level, LT-CTX adaptation correlated with major changes in cell morphology and actin cytoskeleton organization as revealed by E-cadherin (Fig. 6, *upper panels*) and phalloidin (Fig. 6, *lower panels*) staining, respectively. While LT sub-culture with regular medium somewhat induced a mesenchymal-like actin cytoskeleton characterized by the presence of F-actin stress fibers accompanying loss of E-cadherin expression, chronic supplementation with CTX promoted a stable epithelial state, as these cells showed distinct expression of E-cadherin at cell–cell junctions, and corresponding cortical F-actin staining below the cell membranes.

CHRONIC EXPOSURE TO CETUXIMAB PREVENTS DYNAMIC, SPONTANEOUS EMERGENCE OF THE MESENCHYMAL $CD44^{POS}/CD24^{NEG/LOW}$ PHENOTYPE

The EMT process causally participates in the emergence of cancer stem cell-like phenotypes, a prerequisite for cancer cell metastasis. Thus, stem cell-like breast cancer cell populations bearing the mesenchymal $CD44^{pos}CD24^{neg/low}$ immunophenotype strongly express a TGFβ-driven EMT-like pathway signature and become more epithelial-like after TGFβ pathway inhibition [Blick et al., 2010; Chng et al., 2010], providing further evidence for a pivotal role of TGFβ in driving breast cancer EMT and promoting maintenance of cancer stem cells. To explore the possibility that CTX's efficacy may relate to its ability to prevent the occurrence of spontaneous EMT-related differentiation/de-differentiation processes, we tracked the time evolution of phenotypic diversification in CTX-naïve A431 parental cells and LT-CTX-adapted A431 POOLs subpopulations. Fig. 7 shows a summarized time-course analysis of parental A431 cells and LT-CTX-adapted A431 POOLs with respect

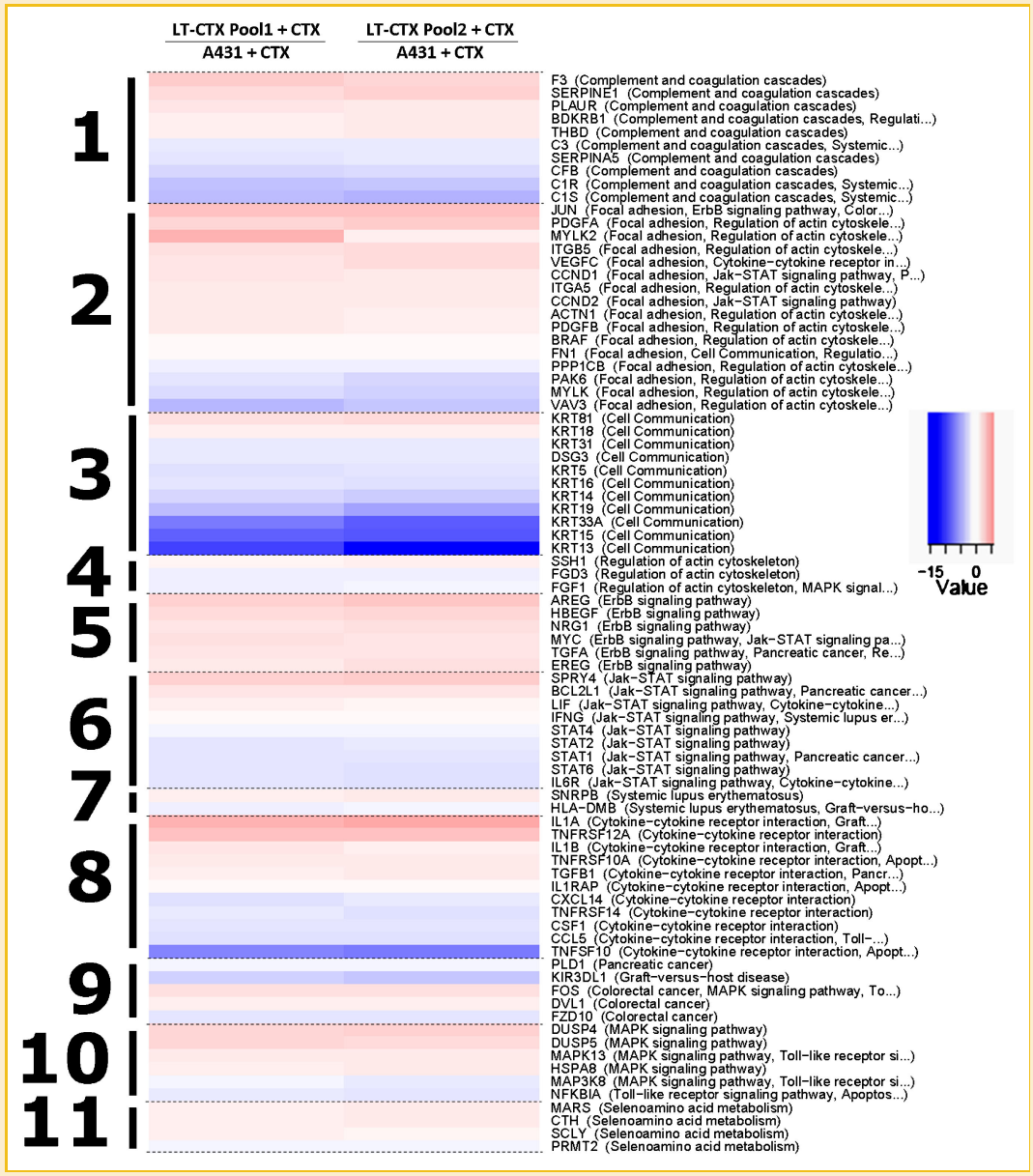

Fig. 4. Characterization of LT-CTX-adapted A431 POOLs relative to parental A431 cells (IV): Pathway-based transcriptomic signature defining CTX's molecular functioning in *EGFR* gene-amplified *KRAS* WT tumor cells. The evolution of predictive biomarkers for CTX efficacy in *KRAS* WT cell-line models was monitored using a pathway-based association analysis of genome-wide screening data as described in the Materials and Methods Section. The heat map shows the (clustered) lists of genes ordered according to significant functions detected by GSEA with KEGG pathways. (1) Complement and Coagulation Cascade; (2) Focal adhesion; (3) Cell Communication; (4) Regulation of Actin Cytoskeleton; (5) ErbB Signaling Pathway; (6) Jak-STAT Signaling Pathway; (7) Systemic Lupus Erythematosus; (8) Cytokine–Cytokine Receptor Interaction; (9) Colorectal Cancer; (10) MAPK Signaling; (11) Selenoamino Acid Metabolism. Expression values are represented as colors, where the range of colors (red, pink, light blue, and dark blue) shows the range of expression values (high, moderate, low, and the lowest, respectively) (CTX, cetuximab).

to four fractions of cell subpopulation as defined by the absence or presence of CD44/CD24 cell surface markers (i.e., $CD44^{pos}/CD24^{neg}$, $CD44^{neg}/CD24^{pos}$, $CD44^{pos}/CD24^{pos}$, and $CD44^{neg}/CD24^{neg}$). Low-passage parental A431 cells were largely positive for both CD24 and CD44 as the basal population was highly enriched with the $CD44^{pos}/CD24^{pos}$ sub-fraction (63%). Interestingly, assessment of the $CD44^{pos}/CD24^{neg/low}$ mesenchymal immunophenotype revealed that the relative enrichment of this sub-population switched with time in A431 WT cells continuously subcultured in regular medium. Thus, a significantly increased subpopulation of A431 cells bearing $CD44^{pos}/CD24^{neg/low}$ could be found after ~8 months. At later passages (>16 months), >90% of A431 cells became $CD44^{pos}/CD24^{neg/low}$ to closely resemble highly $CD44^{pos}/CD24^{neg/low}$-enriched cell number found in cultures of highly-metastatic tumor cells of mesenchymal origin (e.g., MDA-MB-231 basal-like breast cancer cells; Oliveras-Ferraros et al., 2010a). Of note, LT-CTX-adapted A431 POOLs notably down-regulated the parental high-levels of CD44 while increasing their CD24 status when compared to

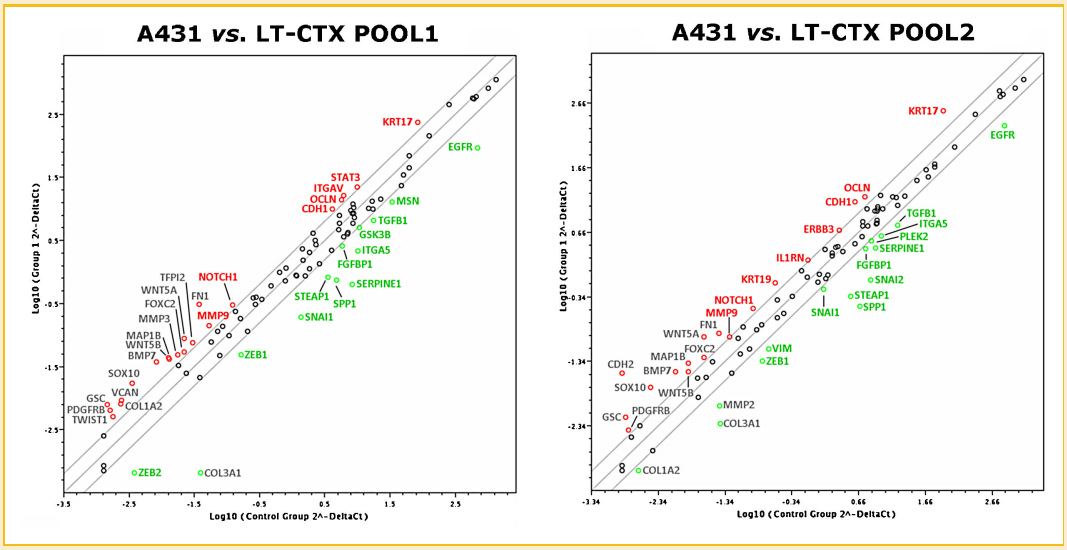

Fig. 5. Characterization of LT-CTX-adapted A431 POOLs relative to parental A431 cells (V): Expression status of the EMT genetic program. Total RNA from parental A431 cells and LT-CTX-adapted A431 POOLs was characterized in technical triplicates using the Human EMT RT^2 Profiler PCR Array as per manufacturer's instructions (SABiosciences). Figures show representative scatter plots of the difference (≥2-fold; green and red symbols: Down- and up-regulation versus basal expression levels in untreated parental A431 cells, respectively) in relative transcript abundance of 84 key genes that either change their expression during the EMT process or regulate those EMT-related gene expression changes.

parental A431 cells. Indeed, LT-CTX-adapted A431 POOLs virtually lacked a CD44^{pos}/CD24$^{neg/low}$ mesenchymal population (i.e., 0% in POOL1 and up to 2% in POOL2 after 16 months of chronic exposure to CTX). Conversely, flow cytometry analyses clearly established that chronic adaptation to CTX was accompanied by a dramatic enrichment (up to 40-fold increase) in A431 cell populations bearing a CD44^{neg}/CD24^{pos} epithelial immunophenotype (from 2% in LT cultured A431 WT cells to 80% in POOL1 and 62% in POOL2 after 16 months of chronic exposure to CTX).

DISCUSSION

A significantly increased presence of epithelial features and a complete prevention of the spontaneous acquisition of mesenchymal features (e.g., stronger E-cadherin and occludin expression, down-regulation of the pivotal epithelial repressors *Zeb*, *Snail*, and *Slug* and significant restoration of cortical F-actin) in our LT culture system of *EGFR* gene-amplified *KRAS* WT A431 epidermoid cancer cells chronically exposed to CTX, support the notion that CTX's molecular functioning largely relates to its ability to prevent the EMT process. The transmembrane proteins E-cadherin and occludin, by functioning as pivotal parts of adherens junctions and tight junctions, respectively, associate with and reorganizes the actin cytoskeleton during formation and maturation of cell–cell contacts [Hartsock and Nelson, 2008]. These findings, along with the transcriptomic signature obtained upon bioinformatic evaluation of multiple genome-wide analyses using GSEA-based screening of the KEGG pathway database, support further the functional relevance of EMT-related *focal adhesion*, *cell communication*, and *regulation of actin cytoskeleton* as pivotal signaling pathways that underlie CTX efficacy. Importantly, our current description of CTX-regulated EMT-related molecular processes appears to specifically relate to CTX's mechanism of action because they took place without altering the mode of action and/or accessibility to other HER1 and/or HER2 inhibitors (i.e., gefitinib, erlotinib, lapatinib, and trastuzumab; Fig. 1).

Given that signaling emanating from focal adhesions, integrins and/or PDGF is required to activate the EMT program in response to TGFβ [Bates, 2005; Gotzmann et al., 2006; Cicchini et al., 2008; Bianchi et al., 2010], and that activation of the EMT program generates migrating cancer stem cells by directly linking the acquisition of cellular motility with the maintenance of tumor-initiating (stemness) capacity [Mani et al., 2008; Morel et al., 2008; Yang and Weinberg, 2008], it could be tempting to suggest that, because its ability to inhibit the EMT genetic program as a core biological network within a larger and complex transcriptomic signature CTX, CTX's efficacy could be measured in terms of its regulatory effect on the balance between self-renewal and differentiation in tumor-initiating cells [Monteiro and Fodde, 2010]. This scenario could provide a molecular linkage to two recent studies by Skvortsova et al. [2010] and Pueyo et al. [2010] that investigated the effects and the mechanism of action of action when combined with radiation. The first revealed that failure of CTX to enhance radiation response in FaDu xenografts associated with the initiation of the EMT program, whereas activation of the reverse MET program was observed in A431 xenografts, which showed increased CTX-caused tumor response to radiation [Skvortsova et al., 2010]. The latter study revealed that maintenance treatment with CTX significantly prevented the occurrence of A431 aggressive phenotypes induced with pre-treatment with fractionated radiotherapy, thus suggesting that CTX maintenance therapy efficiently

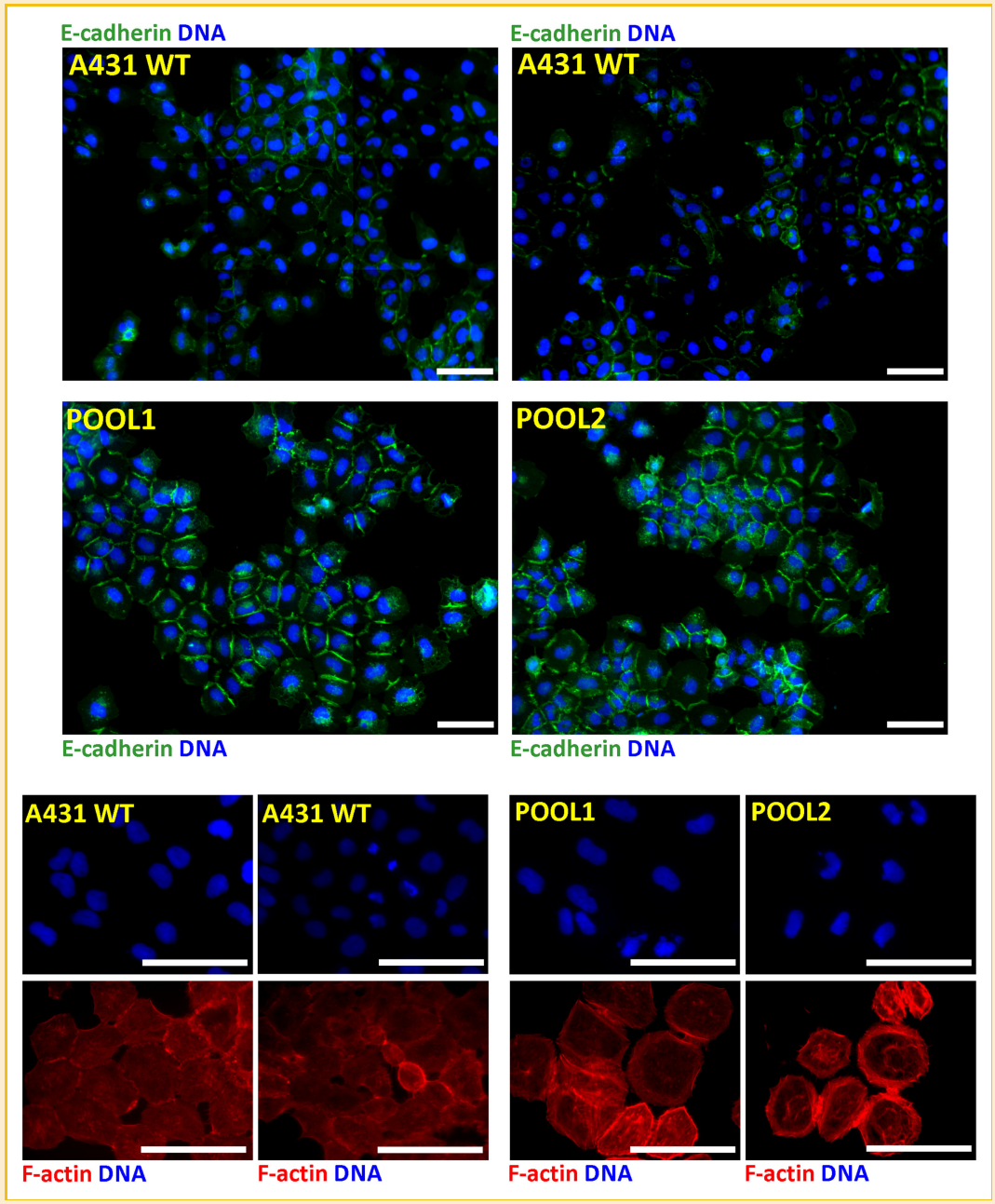

Fig. 6. Characterization of LT-CTX-adapted A431 POOLs relative to parental A431 cells (VI): E-cadherin and cytoskeleton organization. After fixation and permeabilization, cellular distribution of E-cadherin (green staining; upper panels, 4 × 4 montages) and F-actin (red staining; lower panels) was assessed following staining with anti-E-cadherin (1:200 dilution of E-Cadherin [24E10] Rabbit mAb #3195, Cell Signaling Technology, Inc.) and anti-F-actin (1:50 dilution of Alexa Fluor® 594 Phalloidin [A12381; Invitrogen, Carlsbad, CA]) antibodies, as specified, and Hoechst 33258 for nuclear counterstaining (blue). Images show representative whole populations of starting (low-passage) parental A431 cells (top left corner), LT (high-passage) medium-treated A431 cells (top right corner), LT-CTX-adapted A431 POOL1 (bottom left corner), and LT-CTX-adapted A431 POOL2 growing in individual wells that were captured using different channels for E-cadherin (green), F-actin (red) and Hoechst 33258 (blue) with a 20× objective on BD Pathway™ 855 Bioimager System, and merged using BD Attovision™ software. Scale bar = 100 μm.

blocks the expression of factors that promote cell survival and induce an aggressive phenotype in tumor cells surviving radiation [Pueyo et al., 2010]. We have recently learned that modulation of gene regulation mediated by the epithelial transcriptional repressors *Snail* and *Slug* is critical for a cancer cell to acquire stem cell-like characteristics toward resisting radiotherapy (or chemotherapy-) mediated cellular stress [Kurrey et al., 2009]. That is, in response to radiation (and chemotherapy), *Snail/Slug*-overexpressing cancer cells are bestowed with three critical capabilities that define the functionality and survival of metastatic cancer stem cells, namely EMT, resistance to apoptosis, and a self-renewal program. We now reveal that A431 WT cells LT cultured in regular medium can

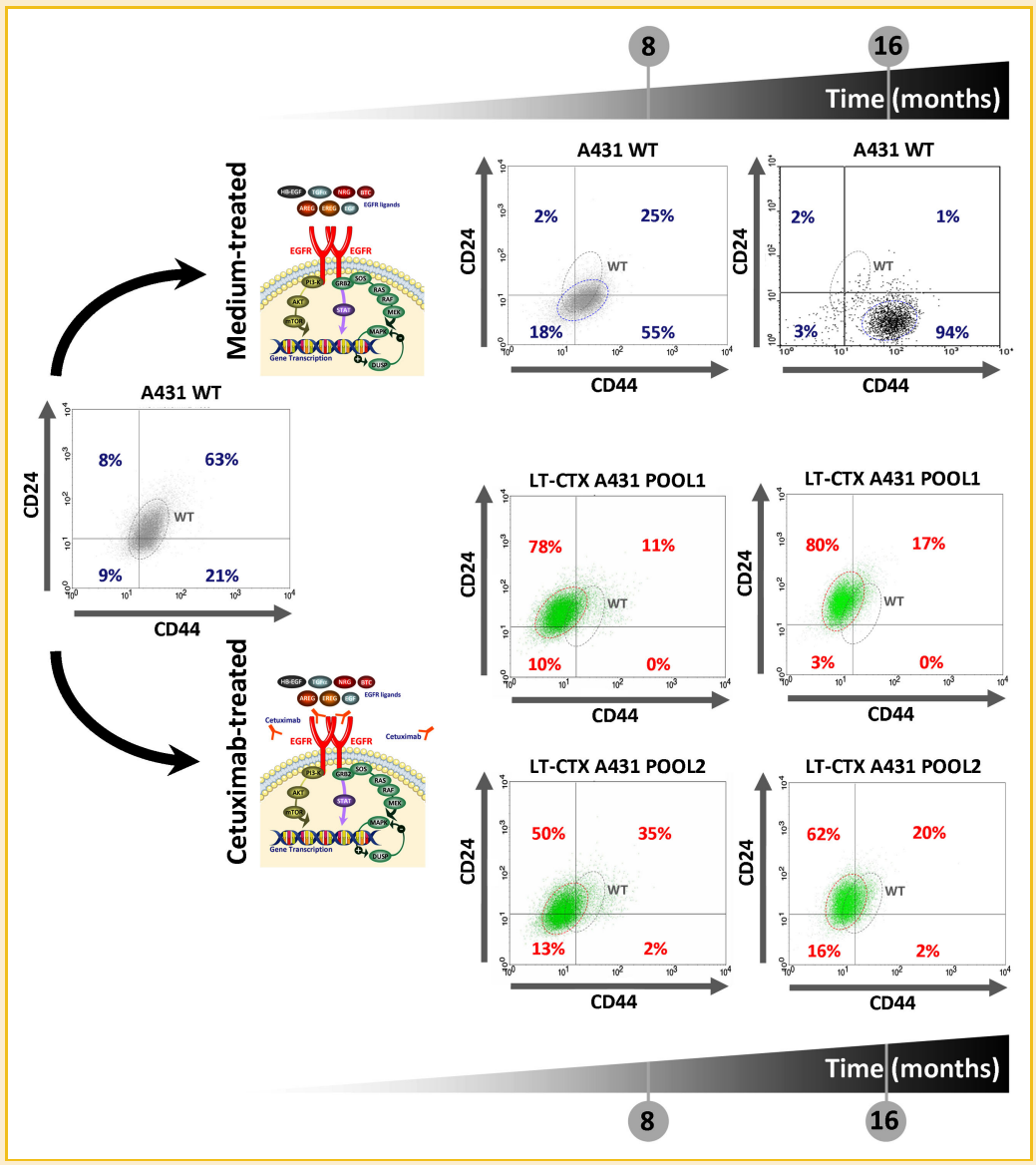

Fig. 7. Characterization of LT-CTX-adapted A431 POOLs relative to parental A431 cells (VII): $CD24^{pos}/CD24^{neg/low}$ mesenchymal immunophenotype. Presented are representative flow cytometry dot plots for the time-course (0, 8, and 16 months) expression of CD44 (X-axis) and CD24 (Y-axis) cell markers in (low-passage) parental A431 cells, LT (high-passage) medium-treated A431 cells, LT-CTX-adapted A431 POOL1 (bottom left corner), and LT-CTX-adapted A431 POOL2, as specified. The results of this analysis are summarized (%) with respect to four cell population fractions: $CD44^{pos}CD24^{neg}$, $CD44^{neg}CD24^{pos}$, $CD44^{pos}CD24^{pos}$, and $CD44^{neg}CD24^{neg}$.

undergo a starling phenotypic diversification compatible with EMT in vitro as defined by decreased E-cadherin expression and disruption of cellular contacts between cells, gain of vimentin expression, and acquisition of mesenchymal-like cellular/morphological alterations. While the starting A431 population mostly displayed epithelial features including tight cell–cell contacts and growth of organized, compact colonies, LT cultivation of parental A431 WT cells significantly increased the number of cells exhibiting a fibroblast-like cell shape growing as singles cells or forming small aggregates. The spontaneous multilineage evolution of a priori cytokeratin- and vimentin-negative parental A431 cells manifested by changes in morphology and in the emergence of distinct cellular subsets expressing exclusive patterns of lineage markers indicative of mesenchymal differentiation has been repeatedly recognized by Milsom et al. [2007, 2008, 2009] in their analyses of A431 tumors in vivo and A431 cell populations in vitro. LT adaptation to CTX, however, completely prevented the molecular mechanisms driving spontaneous EMT in LT cultured A431, which remained in an even enhanced epithelial state. CTX chronic exposure might impede, therefore, the ability of cancer stem cells-like A431 cells to fully assume, in a spontaneous or radiotherapy-/chemotherapy-induced manner, metastasis-facilitating mesenchymal properties [Reya et al., 2001].

If CTX efficacy directly relates to the exacerbated occurrence of subpopulations of tumor cells with features of cancer stem cells and/or the sole presence of stem cell-related features such as the (e.g.,

integrins- and cytokines-driven) capacity to migrate, molecular markers associated with the growth, survival and/or motility of tumor stem/progenitor cells might be need to be prospectively evaluated in *KRAS* WT patient selection for CTX-based therapies. LT incubation of A431 cells with the EGFR ligand EGF causes endocytosis and degradation of the epithelial marker E-cadherin, which is paralleled by induction of the EMT hallmark *Snail* [Lu et al., 2003]. A potential explanation of CTX-prevented EMT lies, therefore, in the capacity of CTX to compete with EGF for binding sites on the EGFR receptor to inhibit the ligand promoting effects on EMT and/or to down-regulate the expression of alternative ligands that can activate EGFR via heterodimerization with other members of the HER family (e.g., HER3, HER4). In this regard, there are few studies suggesting that EGFR ligands such as *AREG* and DUSPs such as *DUSP6* may actively participate in the control of self-renewal and maintenance of stem cell characteristics in several tissues [Li et al., 2007; Booth et al., 2010]. Forthcoming studies should definitely establish whether the molecular behavior of CTX as either ''self-renewal therapy'' (i.e., a blocker of signaling networks implicated in the control of normal and malignant stem cell self-renewal or maintenance) or ''differentiation therapy'' (i.e., an agent that force stem/progenitor cells to differentiate, thereby potentially decreasing self-renewal capacity and rendering them sensitive to systemic therapies) [Liu and Wicha, 2010] may explain the pivotal role of genes belonging to the ErbB (e.g., *AREG, EREG*, and *MYC*), MAPK (e.g., *DUSP4* and *DUSP6*), focal adhesion, cytoskeleton, and cell–cell communication (e.g., *integrins*, *PDGF*, and *keratins*) signaling pathways as activators or mediators of the main intracellular cascades controlling EGFR-regulated cell migration (i.e., the Jak-STAT axis) and EGF-enhanced TGFβ1 activity, both inducing and/or maintaining the EMT status in cancer stem-like cells [Uttamsingh et al., 2008; Wendt et al., 2010].

Because all correlative studies to date have been performed using retrospective analyses, it is obvious that candidate predictive and surrogate molecular markers for CTX benefit -including *KRAS* WT status – need to be prospectively evaluated and validated in patient selection for CTX-based therapies. By tracking the evolution of predictive biomarkers for CTX efficacy after LT CTX treatment of EGFR-positive *KRAS* WT tumor cells using a pathway-based association analysis of genome-wide screening data, we here provide pre-clinical support to the notion that similar molecular mechanisms could underlie both forms of de novo and auto-acquired resistance to CTX [Wheeler et al., 2010]. Therefore, the most significant distinction between intrinsic (primary) and acquired (secondary) CTX refractoriness in *KRAS* WT mCRC patients could be just the timing of detection. Perhaps more importantly, the expression status of *AREG*, *EREG*, and/or *DUSP* mRNAs and its impact in predicting tumor cell response to the growth inhibitory activity of CTX appears to be tightly linked with the simultaneous occurrence of epithelial or mesenchymal phenotypes in target cancer cells. Recent evidence has indicated that the success of HER2-directed therapies such as trastuzumab may be explained, at least in part, by their preferential killing of cancer stem cells in *HER2*-positive carcinomas [Korkaya et al., 2008; Li et al., 2008; Magnifico et al., 2009]. Intriguingly, a variety of possible mechanisms of escape from trastuzumab appear to involve many of the same set of molecular markers that have been implicated in the biology of cancer stem cells [Bedard et al., 2009]. We have recently confirmed that HER2-dependent cancer cells exhibiting de novo or acquired resistance to trastuzumab are significantly enriched with EMT and stem cell-like features [Oliveras-Ferraros et al., 2010a,b; Vazquez-Martin et al., 2010]. If, similarly to the mono-HER2 inhibitor trastuzumab, the efficacy of the mono-HER1 inhibitor CTX largely relates to the degree of reduction and impairment of functional cancer stem cells (e.g., by reversing the EMT to MET phenotype), the feasibility of EMT/MET morphological/molecular profiling in tumor tissues as a potential predictor of response to CTX might be explored with caution in future studies [Arnoletti et al., 2010].

KRAS mutation status is being used as the sole biomarker to predict therapeutic efficiency of CTX mCRC. A significant number of mCRC patients with *KRAS* WT tumors, however, do not benefit from CTX and we are lacking additional predictors in EGFR-dependent carcinomas with either an intact *KRAS* signaling [e.g., HNSCC; Mehra et al., 2008] or in which *KRAS* mutations do not predict CTX efficacy [e.g., NSCLC; Ettinger, 2010]. While *KRAS* mutations account for approximately 30–40% mCRC patients who are not responsive to EGFR-targeted therapies including CTX, we now suggest that not only *BRAF* mutations have a predictive value but also EMT-related molecular changes that could allow either de novo occurrence or the secondary emergence of biologically aggressive cell progenies refractory to CTX in *KRAS* WT patients. Moreover, it should be noted that unlike *EGFR* mutations—which are almost uniformly restricted to NSCLC [Rosell et al., 2010]—and *KRAS* mutations—which are informative of CTX inefficacy solely in mCRC [Weber et al., 2003; Sánchez-Muñoz et al., 2010]—immunohistochemical and/or microarray-based transcriptional profiling studies detecting specific alteration of EMT drivers and/or effectors (i.e., those related to the functioning of CTX against EMT-phenotypic cancer stem-like cells) may be helpful to identify molecular functioning of CTX in cancers in which this EGFR-targeted antibody is widely in clinical use other than CRC (e.g., for locally/regionally advanced HNSCC in combination with radiotherapy and as monotherapy for recurrent/metastatic HNSCC after failing platinum-based chemotherapy). Although in vivo evidence of EMT in tumors has been difficult to obtain likely due to the transient nature of the EMT process and the difficulty of capturing the process in snapshot images of fixed tumor tissue, recent studies combining immunohistochemical staining of positive (e.g., Snail/Zeb), and negative (e.g., E-cadherin/occludin) EMT markers probed to be an efficient approach to identify EMT cells in samples of invasive human ductal breast carcinomas [Vincent et al., 2009; Fuxe et al., 2010]. Future studies using similar staining approaches may be successful in identifying EMT cells (and, therefore, an activation of a cancer stem cell gene signature) in the tumor microenvironment and helpful in classifying responders and nonresponders by determining when and where EMT is induced in tumors being treated with CTX-based therapies.

ACKNOWLEDGMENTS

Alejandro Vazquez-Martin is the recipient of a ''Sara Borrell'' post-doctoral contract (CD08/00283, Ministerio de Sanidad y Consumo,

Fondo de Investigación Sanitaria, FIS, Spain). Work at Menendez' laboratory is supported in part by the Instituto de Salud Carlos III (Ministerio de Sanidad y Consumo, Fondo de Investigación Sanitaria, FIS, Spain, Grants CP05-00090 and PI06-0778 and RD06-0020-0028), the Fundación Científica de la Asociación Española Contra el Cáncer (AECC, Spain), and by the Ministerio de Ciencia e Innovación (SAF2009-11579, Plan Nacional de I+D+I, MICINN, Spain).

REFERENCES

Aoki KF, Kanehisa M. 2005. Using the KEGG database resource. Curr Protoc Bioinformatics (Chapter 1: Unit 1.12).

Arnoletti JP, Frolov A, Eloubeidi M, Keene K, Posey J, Wood T, Greeno E, Jhala N, Varadarajulu S, Russo S, Christein J, Oster R, Buchsbaum DJ, Vickers SM. 2010. A phase I study evaluating the role of the anti-epidermal growth factor receptor (EGFR) antibody cetuximab as a radiosensitizer with chemoradiation for locally advanced pancreatic cancer. Cancer Chemother Pharmacol [Epub ahead of print].

Baker JB, Dutta D, Watson D, Maddala T, Shak S, Rowinsky EK, Xu L, Clark E, Mauro DJ, Khambata-Ford S. 2008. Evaluation of tumor gene expression and K-Ras mutations in FFPE tumor tissue as predictors of response to cetuximab in metastatic colorectal cancer [Abstract]. J Clin Oncol 27(Suppl.): 3512.

Bardelli A, Siena S. 2010. Molecular mechanisms of resistance to cetuximab and panitumumab in colorectal cancer. J Clin Oncol 28:1254–1261.

Bates RC. 2005. Colorectal cancer progression: Integrin alphavbeta6 and the epithelial-mesenchymal transition (EMT). Cell Cycle 4:1350–1352.

Bedard PL, Cardoso F, Piccart-Gebhart MJ. 2009. Stemming resistance to HER-2 targeted therapy. J Mammary Gland Biol Neoplasia 14:55–66.

Bianchi A, Gervasi ME, Bakin AV. 2010. Role of beta5-integrin in epithelial-mesenchymal transition in response to TGFbeta. Cell Cycle 9:1647–1659.

Blick T, Hugo H, Widodo E, Waltham M, Pinto C, Mani SA, Weinberg RA, Neve RM, Lenburg ME, Thompson EW. 2010. Epithelial mesenchymal transition traits in human breast cancer cell lines parallel the CD44(hi/)CD24 (lo/-) stem cell phenotype in human breast cancer. J Mammary Gland Biol Neoplasia 15:235–252.

Booth BW, Boulanger CA, Anderson LH, Jimenez-Rojo L, Brisken C, Smith GH. 2010. Amphiregulin mediates self-renewal in an immortal mammary epithelial cell line with stem cell characteristics. Exp Cell Res 316:422–432.

Chng Z, Teo A, Pedersen RA, Vallier L. 2010. SIP1 mediates cell-fate decisions between neuroectoderm and mesendoderm in human pluripotent stem cells. Cell Stem Cell 6:59–70.

Cicchini C, Laudadio I, Citarella F, Corazzari M, Steindler C, Conigliaro A, Fantoni A, Amicone L, Tripodi M. 2008. TGFbeta-induced EMT requires focal adhesion kinase (FAK) signaling. Exp Cell Res 314:143–152.

Citri A, Yarden Y. 2006. EGF-ERBB signalling: Towards the systems level. Nat Rev Mol Cell Biol 7:505–516.

de Reyniès A, Boige V, Milano G, Faivre J, Laurent-Puig P. 2008. KRAS mutation signature in colorectal tumors significantly overlaps with the cetuximab response signature. J Clin Oncol 26:2228–2230 (author reply: 2230–2231).

De Roock W, Fieuws S, Biesmans B, Jacobs B, De Schutter Y, Humblet Y, Peeters M, Van Cutsem E, Tejpar S. 2009. DUSP expression as a predictor of outcome after cetuximab treatment in Kras wild type and mutant colorectal tumors. ASCO Gastrointestinal Cancers Symposium. Abstract #289.

Ettinger DS. 2010. Emerging profile of cetuximab in non-small cell lung cancer. Lung Cancer 68:332–337.

Freytag J, Wilkins-Port CE, Higgins CE, Higgins SP, Samarakoon R, Higgins PJ. 2010. PAI-1 mediates the TGF-beta1+EGF-induced "scatter" response in transformed human keratinocytes. J Invest Dermatol 130:2179–2190.

Fuxe J, Vincent T, de Herreros AG. 2010. Transcriptional crosstalk between TGFbeta and stem cell pathways in tumor cell invasion: Role of EMT promoting Smad complexes. Cell Cycle 9:2363–2374.

Gattenlöhner S, Etschmann B, Kunzmann V, Thalheimer A, Hack M, Kleber G, Einsele H, Germer C, Müller-Hermelink HK. 2009. Concordance of KRAS/BRAF mutation status in metastatic colorectal cancer before and after anti-EGFR therapy. J Oncol 2009:831626.

Gotzmann J, Fischer AN, Zojer M, Mikula M, Proell V, Huber H, Jechlinger M, Waerner T, Weith A, Beug H, Mikulits W. 2006. A crucial function of PDGF in TGF-beta-mediated cancer progression of hepatocytes. Oncogene 25:3170–3185.

Hartsock A, Nelson WJ. 2008. Adherens and tight junctions: Structure, function and connections to the actin cytoskeleton. Biochim Biophys Acta 1778:660–669.

Hawkes E, Cunningham D. 2010. Relationship between colorectal cancer biomarkers and response to epidermal growth factor receptor monoclonal antibodies. J Clin Oncol 28:e529–e531 (author reply e 532–533).

Hynes NE, Lane HA. 2005. ERBB receptors and cancer: The complexity of targeted inhibitors. Nat Rev Cancer 5:341–354.

Hynes NE, MacDonald G. 2009. ErbB receptors and signaling pathways in cancer. Curr Opin Cell Biol 21:177–184.

Italiano A, Hostein I, Soubeyran I, Fabas T, Benchimol D, Evrard S, Gugenheim J, Becouarn Y, Brunet R, Fonck M, François E, Saint-Paul MC, Pedeutour F. 2010. KRAS and BRAF mutational status in primary colorectal tumors and related metastatic sites: Biological and clinical implications. Ann Surg Oncol 17:1429–1434.

Jacobs B, De Roock W, Piessevaux H, Van Oirbeek R, Biesmans B, De Schutter J, Fieuws S, Vandesompele J, Peeters M, Van Laethem JL, Humblet Y, Pénault-Llorca F, De Hertogh G, Laurent-Puig P, Van Cutsem E, Tejpar S. 2009. Amphiregulin and epiregulin mRNA expression in primary tumors predicts outcome in metastatic colorectal cancer treated with cetuximab. J Clin Oncol 27:5068–5074.

Keise SM. 2008. Dual-specificity MAP kinase phosphatases (MKPs) and cancer. Cancer Metastasis Rev 27:253–261.

Khambata-Ford S, Garrett CR, Meropol NJ, Basik M, Harbison CT, Wu S, Wong TW, Huang X, Takimoto CH, Godwin AK, Tan BR, Krishnamurthi SS, Burris HA III, Poplin EA, Hidalgo M, Baselga J, Clark EA, Mauro DJ. 2007. Expression of epiregulin and amphiregulin and K-ras mutation status predict disease control in metastatic colorectal cancer patients treated with cetuximab. J Clin Oncol 25:3230–3237.

Korkaya H, Paulson A, Iovino F, Wicha MS. 2008. HER2 regulates the mammary stem/progenitor cell population driving tumorigenesis and invasion. Oncogene 27:6120–6230.

Kokkinos MI, Wafai R, Wong MK, Newgreen DF, Thompson EW, Waltham M. 2007. Vimentin and epithelial-mesenchymal transition in human breast cancer – Observations in vitro and in vivo. Cells Tissues Organs 185:191–203.

Kurrey NK, Jalgaonkar SP, Joglekar AV, Ghanate AD, Chaskar PD, Doiphode RY, Bapat SA. 2009. Snail and slug mediate radioresistance and chemoresistance by antagonizing p53-mediated apoptosis and acquiring a stem-like phenotype in ovarian cancer cells. Stem Cells 27:2059–2068.

Li C, Scott DA, Hatch E, Tian X, Mansour SL. 2007. Dusp6 (Mkp3) is a negative feedback regulator of FGF-stimulated ERK signaling during mouse development. Development 134:167–176.

Li X, Lewis MT, Huang J, Gutierrez C, Osborne CK, Wu MF, Hilsenbeck SG, Pavlick A, Zhang X, Chamness GC, Wong H, Rosen J, Chang JC. 2008. Intrinsic resistance of tumorigenic breast cancer cells to chemotherapy. J. Natl Cancer Inst 100:672–679.

Linardou H, Dahabreh IJ, Kanaloupiti D, Siannis F, Bafaloukos D, Kosmidis P, Papadimitriou CA, Murray S. 2008. Assessment of somatic k-RAS mutations as a mechanism associated with resistance to EGFR-targeted agents: A systematic review and meta-analysis of studies in advanced non-small-cell lung cancer and metastatic colorectal cancer. Lancet Oncol 9:962–972.

Liu S, Wicha MS. 2010. Targeting breast cancer stem cells. J Clin Oncol 28:4006–4012.

Lu Y, Li X, Liang K, Luwor R, Siddik ZH, Mills GB, Mendelsohn J, Fan Z. 2007. Epidermal growth factor receptor (EGFR) ubiquitination as a mechanism of acquired resistance escaping treatment by the anti-EGFR monoclonal antibody cetuximab. Cancer Res 67:8240–8247.

Lu Z, Ghosh S, Wang Z, Hunter T. 2003. Downregulation of caveolin-1 function by EGF leads to the loss of E-cadherin, increased transcriptional activity of beta-catenin, and enhanced tumor cell invasion. Cancer Cell 4:499–515.

Magnifico A, Albano L, Campaner S, Delia D, Castiglioni F, Gasparini P, Sozzi G, Fontanella E, Menard S, Tagliabue E. 2009. Tumor-initiating cells of HER2-positive carcinoma cell lines express the highest oncoprotein levels and are sensitive to trastuzumab. Clin Cancer Res 15:2010–2021.

Mandic R, Rodgarkia-Dara CJ, Zhu L, Folz BJ, Bette M, Weihe E, Neubauer A, Werner JÁ. 2006. Treatment of HNSCC cell lines with the EGFR-specific inhibitor cetuximab (Erbitux) results in paradox phosphorylation of tyrosine 1173 in the receptor. FEBS Lett 580:4793–4800.

Massagué J. 2008. TGFbeta in cancer. Cell 134:215–230.

Mani SA, Guo W, Liao MJ, Eaton EN, Ayyanan A, Zhou AY, Brooks M, Reinhard F, Zhang CC, Shipitsin M, Campbell LL, Polyak K, Brisken C, Yang J, Weinberg RA. 2008. The epithelial-mesenchymal transition generates cells with properties of stem cells. Cell 133:704–715.

Mehra R, Cohen RB, Burtness BA. 2008. The role of cetuximab for the treatment of squamous cell carcinoma of the head and neck. Clin Adv Hematol Oncol 6:742–750.

Milsom C, Anderson GM, Weitz JI, Rak J. 2007. Elevated tissue factor procoagulant activity in CD133-positive cancer cells. J Thromb Haemost 5:2550–2552.

Milsom CC, Yu JL, Mackman N, Micallef J, Anderson GM, Guha A, Rak JW. 2008. Tissue factor regulation by epidermal growth factor receptor and epithelial-to-mesenchymal transitions: Effect on tumor initiation and angiogenesis. Cancer Res 68:10068–10076.

Milsom C, Magnus N, Meehan B, Al-Nedawi K, Garnier D, Rak J. 2009. Tissue factor and cancer stem cells: Is there a linkage? Arterioscler Thromb Vasc Biol 29:2005–2014.

Monteiro J, Fodde R. 2010. Cancer stemness and metastasis: Therapeutic consequences and perspectives. Eur J Cancer 46:1198–1203.

Morel AP, Lièvre M, Thomas C, Hinkal G, Ansieau S, Puisieux A. 2008. Generation of breast cancer stem cells through epithelial-mesenchymal transition. PLoS One 3:e2888.

Moreno-Bueno G, Portillo F, Cano A. 2008. Transcriptional regulation of cell polarity in EMT and cancer. Oncogene 27:6958–6969.

Moreno-Bueno G, Peinado H, Molina P, Olmeda D, Cubillo E, Santos V, Palacios J, Portillo F, Cano A. 2009. The morphological and molecular features of the epithelial-to-mesenchymal transition. Nat Protoc 4:1591–1613.

Moustakas A, Heldin CH. 2007. Signaling networks guiding epithelial-mesenchymal transitions during embryogenesis and cancer progression. Cancer Sci 98:1512–1520.

Oliveras-Ferraros C, Vazquez-Martin A, López-Bonet E, Martín-Castillo B, Del Barco S, Brunet J, Menendez JA. 2008. Growth and molecular interactions of the anti-EGFR antibody cetuximab and the DNA cross-linking agent cisplatin in gefitinib-resistant MDA-MB-468 cells: New prospects in the treatment of triple-negative/basal-like breast cancer. Int J Oncol 33:1165–1176.

Oliveras-Ferraros C, Vazquez-Martin A, Martin-Castillo B, Cufí S, Del Barco S, Lopez-Bonet E, Brunet J, Menendez JA. 2010a. Dynamic emergence of the mesenchymal CD44(pos)CD24(neg/low) phenotype in HER2-gene amplified breast cancer cells with de novo resistance to trastuzumab (Herceptin). Biochem Biophys Res Commun 397:27–33.

Oliveras-Ferraros C, Vazquez-Martin A, Martin-Castilló B, Pérez-Martínez MC, Cufí S, Del Barco S, Bernado L, Brunet J, López-Bonet E, Menendez JA. 2010b. Pathway-focused proteomic signatures in HER2-overexpressing breast cancer with a basal-like phenotype: New insights into de novo resistance to trastuzumab (Herceptin). Int J Oncol 37:669–678.

Paccione RJ, Miyazaki H, Patel V, Waseem A, Gutkind JS, Zehner ZE, Yeudall WA. 2008. Keratin down-regulation in vimentin-positive cancer cells is reversible by vimentin RNA interference, which inhibits growth and motility. Mol Cancer Ther 7:2894–2903.

Peinado H, Olmeda D, Cano A. 2007. Snail, Zeb and bHLH factors in tumour progression: An alliance against the epithelial phenotype? Nat Rev Cancer 7:415–428.

Pueyo G, Mesia R, Figueras A, Lozano A, Baro M, Vazquez S, Capella G, Balart J. 2010. Cetuximab may inhibit tumor growth and angiogenesis induced by ionizing radiation: A preclinical rationale for maintenance treatment after radiotherapy. Oncologist 15:976–986.

Reya T, Morrison SJ, Clarke MF, Weissman IL. 2001. Stem cells, cancer, and cancer stem cells. Nature 414:105–111.

Rosell R, Morán T, Carcereny E, Quiroga V, Molina MA, Costa C, Benlloch S, Tarón M. 2010. Non-small-cell lung cancer harbouring mutations in the EGFR kinase domain. Clin Transl Oncol 12:75–80.

Samarakoon R, Higgins CE, Higgins SP, Higgins PJ. 2009. TGF-beta1-induced expression of the poor prognosis SERPINE1/PAI-1 gene requires EGFR signaling: A new target for anti-EGFR therapy. J Oncol 2009:342391.

Sánchez-Muñoz A, Gallego E, de Luque V, Pérez-Rivas LG, Vicioso L, Ribelles N, Lozano J, Alba E. 2010. Lack of evidence for KRAS oncogenic mutations in triple-negative breast cancer. BMC Cancer 10:136.

Santini D, Spoto C, Loupakis F, Vincenzi B, Silvestris N, Cremolini C, Canestrari E, Graziano F, Galluccio N, Salvatore L, Caraglia M, Zito FA, Colucci G, Falcone A, Tonini G, Ruzzo A. 2010. High concordance of BRAF status between primary colorectal tumours and related metastatic sites: Implications for clinical practice. Ann Oncol 21:1565.

Siena S, Sartore-Bianchi A, Di Nicolantonio F, Balfour J, Bardelli A. 2009. Biomarkers predicting clinical outcome of epidermal growth factor receptor-targeted therapy in metastatic colorectal cancer. J Natl Cancer Inst 101:1308–1324.

Singh A, Settleman J. 2010. EMT, cancer stem cells and drug resistance: An emerging axis of evil in the war of cancer. Oncogene 29:4741–4751.

Skvortsova I, Skvortsov S, Raju U, Stasyk T, Riesterer O, Schottdorf EM, Popper BA, Schiestl B, Eichberger P, Debbage P, Neher A, Bonn GK, Huber LA, Milas L, Lukas P. 2010. Epithelial-to-mesenchymal transition and c-myc expression are the determinants of cetuximab-induced enhancement of squamous cell carcinoma radioresponse. Radiother Oncol 96:108–115.

Smith G, Bounds R, Wolf H, Steele RJ, Carey FA, Wolf CR. 2010. Activating K-Ras mutations outwith 'hotspot' codons in sporadic colorectal tumours – Implications for personalised cancer medicine. Br J Cancer 102:693–703.

Subramanian A, Tamayo P, Mootha VK, Mukherjee S, Ebert BL, Gillette MA, Paulovich A, Pomeroy SL, Golub TR, Lander ES, Mesirov JP. 2005. Gene set enrichment analysis: A knowledge-based approach for interpreting genome-wide expression profiles. Proc Natl Acad Sci USA 102:15545–15550.

Thiery JP, Acloque H, Huang RY, Nieto MA. 2009. Epithelial-mesenchymal transitions in development and disease. Cell 139:871–890.

Uttamsingh S, Bao X, Nguyen KT, Bhanot M, Gong J, Chan JL, Liu F, Chu TT, Wang LH. 2008. Synergistic effect between EGF and TGF-beta1 in inducing oncogenic properties of intestinal epithelial cells. Oncogene 27:2626–2634.

Vazquez-Martin A, Oliveras-Ferraros C, Barco SD, Martin-Castillo B, Menendez JA. 2010. The anti-diabetic drug metformin suppresses self-renewal and proliferation of trastuzumab-resistant tumor-initiating breast cancer stem cells. Breast Cancer Res Treat [Epub ahead of print].

Viloria-Petit A, Crombet T, Jothy S, Hicklin D, Bohlen P, Schlaeppi JM, Rak J, Kerbel RS. 2001. Acquired resistance to the antitumor effect of epidermal growth factor receptor-blocking antibodies in vivo: A role for altered tumor angiogenesis. Cancer Res 61:5090–5101.

Vincent T, Neve EP, Johnson JR, Kukalev A, Rojo F, Albanell J, Pietras K, Virtanen I, Philipson L, Leopold PL, Crystal RG, de Herreros AG, Moustakas A, Pettersson RF, Fuxe J. 2009. A SNAIL1-SMAD3/4 transcriptional repressor complex promotes TGF-beta mediated epithelial-mesenchymal transition. Nat Cell Biol 11:943–950.

Weber A, Langhanki L, Sommerer F, Markwarth A, Wittekind C, Tannapfel A. 2003. Mutations of the BRAF gene in squamous cell carcinoma of the head and neck. Oncogene 22:4757–4759.

Wendt MK, Smith JA, Schiemann WP. 2010. Transforming growth factor-beta-induced epithelial-mesenchymal transition facilitates epidermal growth factor-dependent breast cancer progression. Oncogene [Epub ahead of print].

Wharton K, Derynck R. 2009. TGFbeta family signaling: Novel insights in development and disease. Development 136:3691–3697.

Wheeler DL, Dunn EF, Harari PM. 2010. Understanding resistance to EGFR inhibitors-impact on future treatment strategies. Nat Rev Clin Oncol 7:493–507.

Wong R, Cunningham D. 2008. Using predictive biomarkers to select patients with advanced colorectal cancer for treatment with epidermal growth factor receptor antibodies. J Clin Oncol 26:5668–5670.

Yang J, Weinberg RA. 2008. Epithelial–mesenchymal transition: At the crossroads of development and tumor metastasis. Dev Cell 14:818–829.

Yoshida T, Okamoto I, Okabe T, Iwasa T, Satoh T, Nishio K, Fukuoka M, Nakagawa K. 2008. Matuzumab and cetuximab activate the epidermal growth factor receptor but fail to trigger downstream signaling by Akt or Erk. Int J Cancer 122:1530–1538.